OPTICAL AND ION ENERGY SPECTROSCOPY OF LASER-PRODUCED PLASMAS

by

Gregory John Tallents

A thesis submitted for the degree of
Doctor of Philosophy at the
Australian National University

Canberra

January 1978

PREFACE

All the theoretical computations and experimental observations presented in this thesis have been carried out by the author, with the exception of the luminosity time-of-flight measurements (Section 6.2.2). One of the computer codes developed is of general interest and has been published (1). The principal theoretical results have been reported in (2) and (3). The electrostatic analyzer, constructed in the Laboratory Workshop of the Research School and set-up by the author, has been described, along with results on space charge effects, in (4).

I have followed the usual practice in the literature on the choice of units. Consequently, Chapters 2 and 3 and Appendix A are in CGS units, while Chapters 4, 5 and 6, and Appendix B are in SI units. Throughout, much use is made of the electron volt (eV) as a measure of temperature (1 eV = 11605 °K).

I am indebted to many people in the School and Department for their assistance. In particular, it is a pleasure to acknowledge Dr F E Irons for his excellent supervision of the project and helpful advice throughout, and for his critical reading of my papers and this manuscript. I also thank Dr G B Gillman for his help in operating the laser, and for the many improvements made

to the laser, and thank Dr B Luther-Davies, Dr J L Hughes, Dr M J Hollis (of the Department of Engineering Physics), Dr R L Dewar (formerly of the Department of Theoretical Physics, now at Princeton University), and Dr K V Roberts (visitor to the Department of Theoretical Physics, permanently at Culham Laboratory) for their assistance.

The excellent technical support in the School generally, and in the Department of Engineering Physics specifically is acknowledged. The assistance of Mr K G Renner in the setting-up of my experiment has been particularly helpful. The day-to-day maintenance of the laser was performed by Dr G B Gillman, Mr L J Allinson and Mr L Dowen. Mr D Barrott (Drafting Office, Engineering Physics), Mr G R Jones, Mr A R Reading (both of the Laboratory Workshop) and Mr P A Smith (Electronics) were responsible for the engineering design and construction of the analyzer. I particularly thank Mr D Barrott for the slit mechanism design (Appendix B).

I am grateful to Professor S. Kaneff for the opportunity to work in the Department of Engineering Physics. Personal financial support in the form of a Commonwealth Postgraduate Scholarship, and the assistance of the Australian Institute of Nuclear Science and Engineering in equipment purchases is acknowledged.

I thank Mrs M Henderson for typing the manuscript.

January 1978

G J Tallents
Laser Physics Group
Department of Engineering Physics
Research School of Physical Sciences
Australian National University

References

(1) G J Tallents 1976 Comp. Phys. Comm. 12 205-212

'COLLRAD: a code for calculating the quasi-steady state population densities of excited states of hydrogen-like ions'

(2) G J Tallents 1977 J. Phys. B: Atom. Molec. Phys. 10 1769-80

'Population inversions for soft X-ray transitions computed for rapidly cooling plasmas'

(3) G J Tallents 1978 J. Phys. B: Atom. Molec. Phys. submitted for publication

'The effect of Lyman α self-absorption on population inversions between quantum states 2 and 3 of hydrogen-like ions in recombining plasmas'

(4) G J Tallents 1978 J. Phys. E: Sci. Instrum. submitted for publication

'The operation of a 45° parallel plate electrostatic analyzer in laser-produced plasma studies'

ABSTRACT

The work described in this thesis relates to the problem of observing population inversions in laser-produced plasmas, and to the associated problem of interpreting optically thick line intensities.

In Part I we examine the conditions under which population inversions appropriate to soft X-ray transitions can occur in rapidly recombining plasmas, with particular reference to hydrogen-like transitions in a laser-produced carbon plasma. Computations have been performed for quasi-steady state inversions between excited states of hydrogen-like ions, as well as for inversions with respect to the ground state. The effect of Lyman α self-absorption in reducing population inversions between quantum states $n = 2$ and 3 is examined in some detail.

The emergent intensities of optically thick lines from an expanding plasma, such as a laser-produced plasma, are affected by the differential Doppler effect associated with ion streaming. As a first step in investigating this effect we have measured (in Part II) the velocity spectra of the streaming ions. A plasma was produced by focusing the pulse (4 ns duration) from a Neodymium laser onto a carbon target (power density in the range 3×10^{15} to 1.3×10^{16} Wm^{-2}) in vacuum. A 45° parallel plate electrostatic analyzer was built to record the energy spectra of the streaming ions. Space charge effects within the analyzer are examined quantitatively. Ion velocity spectra, deduced from the energy spectra and covering the range $1\text{-}5 \times 10^5$ ms^{-1}, are reported for C^{3+}, C^{4+}, C^{5+} and C^{6+}. The role of recombination in forming these spectra is discussed.

CONTENTS

Page

APPENDICES

CHAPTER 1

INTRODUCTION

When a high power laser pulse is focussed onto a solid target in vacuo a plasma of high electron density (10^{25} - 10^{29} m^{-3}) and temperature (10^{2} - 10^{4} eV) is formed. Subsequent expansion of the plasma into the vacuum environment is accompanied by the ions acquiring directed velocities in excess of 10^{5} ms^{-1}, and by a rapid decrease of density and temperature such that gross departures from local thermal equilibrium (including population inversion) occur.

In order to understand the mechanisms of plasma production, heating, and expansion in laser-produced plasmas, different experimental techniques have been used. Some of the first investigations dealt with the final kinetic energy of the evaporated ions, determined either by time-of-flight measurements (eg Linlor 1963, Gregg and Thomas 1965, Opower and Burlefinger 1965, Opower and Press 1966), electrostatic analyzers (eg Langer et al. 1966, Paton and Isenor 1968), or retarding potentials (eg Honig 1963, Demtröder and Jantz 1970). Laser-produced plasmas were also studied using, for example, high speed photography (eg Ready 1963, Basov et al. 1967), interferometry (eg Bruce et al. 1966, David 1967) and optical spectroscopy (see a list of early references in Boland et al. 1968).

Extensive theoretical and experimental studies of laser-produced plasmas have been prompted, apart from the intrinsic interest in plasmas of such high density, by their possible application as a source of fusion power (eg Nuckolls et al. 1972), as a source of highly charged ions for use with particle accelerators (eg Peacock and Pease 1969, Tonon 1972), by their proven application as a light source for the study of spectra of highly stripped ions (eg Fawcett et al. 1971, 1974), and by their possible application as a source for an X-ray laser. An X-ray laser would open new fields of investigation (Chapline and Wood 1975); for example, holography of crystal structures and biological macromolecules, and the possibility of very fast time resolution. Many different sources have been considered as candidates for an X-ray laser, and there are several review papers of the literature (Bushuev and Kuz'min 1975, Gudzenko et al. 1975, Chapline and Wood 1976, Jaeglé et al. 1976, Waynant and Elton 1976).

In Part I of this thesis we examine, theoretically, the production of population inversions appropriate to X-ray wavelengths in laser-produced plasmas, with particular reference to the hydrogen-like C^{5+} ion. We calculate the necessary cooling rates to achieve population inversions with respect to the ground state, and relate the results to cooling rates in laser-produced plasmas close to the target as predicted by (i) the one-dimensional numerical code MEDUSA, and (ii) a simple model of cooling at the centre

of an expanding plasma (Chapter 2). The effect of Lyman α self-absorption on quasi-steady state population inversions between quantum states n = 2 and 3 of hydrogen-like ions is also investigated (Chapter 3). Appendix A describes the computer code COLLRAD which was devised to calculate the hydrogen-like ion quasi-steady state population densities.

Spectroscopic observations on laser-produced plasmas are usually performed transversely to the axis of expansion (eg Fawcett 1971, Donaldson et al. 1973, Irons and Peacock 1974b). Associated with a differential in the transverse component of ion streaming velocity, there is a differential Doppler effect which complicates the interpretation of emergent, optically thick line intensities (Irons 1975, 1976), and is likely to complicate the detection of population inversions. As a first step towards deducing the Doppler effect, we have constructed (see Part II of this thesis) a 45° parallel plate electrostatic analyzer to record the ion energy spectra of streaming ions (the analyzer is described in Chapter 4). Particular attention has been given to the problem of space charge effects in the analyzer (Chapter 5). Ion energy spectra are presented and analyzed, with particular reference to the effect of recombination (Chapter 6). Appendix B describes an adjustable slit mechanism used to vary the entrance and exit slit widths of the analyzer.

The work described in this thesis is part of an ongoing program in this laboratory on the spectroscopy of laser-produced plasmas. The work of Part I will provide a guide, during the analysis of spectral line intensities, in the quest for population inversions appropriate to soft X-ray wavelengths. Measurements of the ion velocity spectra in Part II, when performed at a number of angles to the target normal, will provide information on the differential in the transverse Doppler effect which is needed to interpret optically thick line intensities, not only in the search for population inversions, but also in the more routine determination of plasma parameters.

PART I

CHAPTER 2

POPULATION INVERSION OF EXCITED QUANTUM STATES WITH RESPECT TO THE GROUND STATE

2.1 Introduction

Calculations based on a quasi-steady-state model for excited quantum states have predicted population inversions between excited states of hydrogen and hydrogen-like ions in recombining plasmas (e.g. Gudzenko and Shelepin 1965, Bohn 1971, 1974; and see Chapter 3). Experimental evidence has also been presented for inversions between excited states of hydrogen in plasma jets (Gol'dfarb and Luk'yanov 1969, Hoffmann and Bohn 1972), between excited states of hydrogen-like ions in laser-produced plasmas (Irons and Peacock 1974, Dewhurst *et al.* 1976), and between excited states of hydrogen and hydrogen-like ions in a magnetic confinement device (Suckewer *et al.* 1976). However, the inversion densities which can be obtained for inversions between quantum states which are quasi-steady state are limited in magnitude because such inversions require that the rate of collisional de-excitation becomes smaller than the rate of radiative de-excitation (for hydrogen-like ions, for example, this only occurs at electron densities less than $Z^7 \times 10^{15}$ cm^{-3}, see Bohn 1974).

Larger inversion densities, for inversions between excited states and with respect to the ground state, are

predicted in rapidly recombining plasmas prior to the establishment of a quasi-steady state. Quantum-state densities, calculated on a time-dependent basis for a hydrogen plasma in which the electron temperature is assumed to decrease instantaneously, show inversions in hydrogen between excited states (Ali and Jones 1976), and with respect to the ground state (Gordiets *et al.* 1968). Similar results have been obtained for hydrogen-like ions (Jones and Ali 1975). In practice, plasmas do not cool instantaneously, and this chapter provides answers to the questions of just how fast a hydrogen-like plasma must cool to yield inversions with respect to the ground state, and whether such cooling rates are practicable in laser-produced plasmas.

The one-dimensional numerical code MEDUSA (Christiansen *et al.* 1974) and a simple model of cooling at the centre of an expanding plasma have been utilized to consider the question of practicability.

2.2 Theory

Consider a plasma composed of hydrogen-like ions, fully stripped ions and electrons. The rate of change of number density N_n (cm^{-3}) of quantum state n of the hydrogen-like ions due to atomic processes is given by

$$\frac{dN_n}{dt} = -N_n \left[N_e \left(K(n,c) + \sum_{m \neq n} K(n,m) \right) + \sum_{m<n} \Lambda(n,m) A(n,m) \right]$$

$$+ N_e \sum_{m \neq n} N_m K(m,n) + \sum_{m>n} N_m \Lambda(m,n) A(m,n) + N_e N^z [K(c,n) + \beta(n)] \qquad (2.1)$$

Here,

N^z (cm^{-3})	denotes the number density of the fully stripped ion
N_e (cm^{-3})	denotes the free-electron density
$A(n,m)$ (s^{-1})	denotes the radiative transition probability from state $n \rightarrow m$
$\Lambda(n,m)$	is the optical escape factor (e.g. Drawin 1970) for the transition $n \rightarrow m$ (this factor allows for self-absorption ($\Lambda < 1$))
$\beta(n)$ $(cm^3 s^{-1})$	denotes the two-body recombination coefficient to the state n
$K(n,m)$ $(cm^3 s^{-1})$	denotes the rate coefficient for the collision-induced transition from state $n \rightarrow m$
$K(c,n)$ and $K(n,c)$ $(cm^3 s^{-1})$	denote the rate coefficients for three-body recombination and collisional ionization respectively, between the continuum c and the state n.

We consider plasmas where the above collisional and radiative processes can be assumed to be the only mechanisms whereby quantum-state densities vary with time (see Section 2.4 for proposed plasmas where this should apply). The solution of equation (2.1) then gives values of N_n (as a function of time) which we can identify with practical values.

We solved equation (2.1) numerically for $N_n (n = 1, 2, 3, \ldots, 20)$ using the expressions for the rate coefficients given in or cited by Bates *et al.* (1962). Regarding the choice of collisional rate coefficients, we note that the rate coefficients of Bates *et al.* do not produce results identical with the hydrogen-like results listed

by them. In their calculations, Bates *et al.* in fact used the collisional rate coefficients for transitions between state n = 1 and states n = 2, 3, 4 and the continuum as listed later in McWhirter and Hearn (1963), although this was not stated in the Bates *et al.* paper (personal communication from Dr R.W.P. McWhirter, and note the misprints: in McWhirter and Hearn, $Z^3K(1,4)$ at θ = 32 000 °K should read 7.44×10^{-11} cm^3s^{-1}; and in Bates *et al.* $Xn_s(1)/Z^{11}$ at θ = 32 000 °K, $\eta(c) = 10^{13}$ cm^{-3} should read 5.5×10^9 cm^{-3}).

The optical escape factors $\Lambda(n,m)$ are equated to unity for all n,m (i.e. all lines optically thin) in most of our calculations, except for some results of figures 2.1 and 2.3 where we set $\Lambda(2,1) = 0.1$ (i.e. 90% self-absorption of L_α).

2.2.1 At time t = 0

We assume at time t = 0 that the plasma is in a steady state ($dN_n/dt = 0$ for all n), in which case the ratio of the fully stripped ion number density to the hydrogen-like ion ground density (N^z/N_1, termed the fractional ionization by Griem 1964) is related to the electron temperature T_e (eV) and density as derived during the course of the present calculations and shown in Figure 2.1. We see in this figure the coronal regime at low density, where N^z/N_1

is independent of density, and the Saha regime at high density, where N^z/N_1 decreases with increasing N_e.

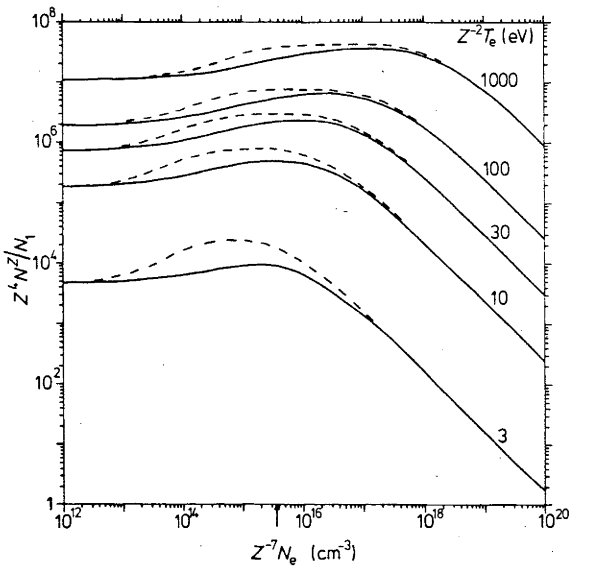

Figure 2.1: Reduced fractional ionization (Z^4N^z/N_1) as a function of reduced electron density ($Z^{-7}N_e$) for steady-state plasmas at various reduced electron temperatures ($Z^{-2}T_e$) as derived during the course of the present calculations. The arrow indicates the reduced density for carbon (Z = 6) when N_e = 10^{21} cm^{-3}. Full curves, optically thin plasma; broken curves, 90% self-absorption of L_α.

A steady-state plasma has been shown to be the most favourable (physically possible) initial state from which to initiate rapid cooling to produce inversions (Green and Silfvast 1976). For hydrogen-like carbon with T_e = 200 eV, N_e = 10^{21} cm^{-3} (values considered in Section 2.3) a steady state can be achieved in the ground-state relaxation time of about 10^{-11} s (substitute into equation (10) of McWhirter and Hearn 1963). This compares with the

cooling time of approximately 10^{-12} s which we will show (see Section 2.3.4) is needed to obtain inversions with respect to the ground state.

2.2.2 At times t > 0

At times t > 0 we assume T_e decreases exponentially with a half-life $T_{1/2}$, while N_e remains constant. (Results in Section 2.4.1, calculated using the MEDUSA code, show that initially the central region of a small expanding sphere cools approximately exponentially with constant N_e.) The calculation of N_n proceeds by the simultaneous solution of equations (2.1) (one equation for each bound state). Following Bates *et al.* (1962), the number of equations to be solved is made finite by assuming that N_n for $n > 20$ is equal to the Saha-Boltzmann value. Population densities for states $n^* < n \leq 20$ are assumed to be quasi-steady state, and for $n \leq n^*$ are calculated on a time-dependent basis. The level n^* is determined by the requirement that the relaxation times of states $n > n^*$ be smaller than about $0.1 \times T_{1/2}$.

The simple Euler method of solving equation (2.1) ($1 \leq n \leq n^*$) was used with iteration at each time-step until values of $N_n (n \leq n^*)$ were obtained within 0.1% of the previous iteration-cycle value. N^z was also obtained iteratively at each time-step by (i) summing N_n up to the highest discrete state as determined by the Debye formula (see Marr 1968), and (ii) applying the condition of charge neutrally. We set

at least 100 time-steps per $T_{1/2}$ value, thus giving at least 10 steps per relaxation time for states $n \leq n^*$. Check calculations using smaller time-steps gave the same results.

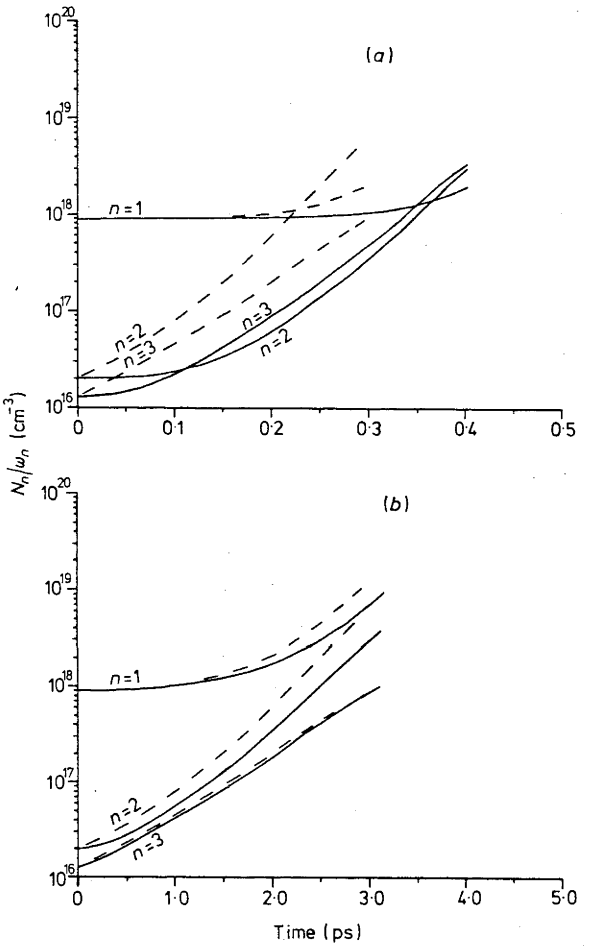

Figure 2.2: The time history of population densities N_n/ω_n (n = 1, 2 and 3) for an optically thin hydrogen-like carbon plasma which is initially in a steady state with T_e = 200 eV and $N_e = 10^{21}$ cm^{-3}, and in which T_e subsequently decreases exponentially with a half-life of (a) 0.1 ps or (b) 1.0 ps while N_e remains constant. The full curves correspond to (a) n* = 5 and (b) n* = 3 (n* is defined in Section 2.2.2). The broken curves, corresponding to n* = 1, are included for comparison.

2.3 Computations

2.3.1 The need for time-dependent computations

Figure 2.2 shows the time history of population densities N_n/ω_n (where $\omega_n = 2n^2$ is the statistical weight of state n) for an optically thin hydrogen-like carbon plasma where $N_e = 10^{21}$ cm^{-3} and where T_e, initially equal to 200 eV, decreases exponentially with $T_{1/2} = 0.1$ ps (Figure 2.2(a)) and $T_{1/2} = 1.0$ ps (Figure 2.2(b)). The full curves, obtained with (a) $n^* = 5$ and (b) $n^* = 3$, are significantly different from the broken curves obtained with $n^* = 1$ when $T_{1/2} = 0.1$ ps, but are comparable with the broken curves when $T_{1/2} = 1.0$ ps. This illustrates the need to calculate the lower excited-state densities on a time-dependent basis when $T_{1/2}$ is as short as 0.1 ps.

Figure 2.2 exemplifies the result, pointed out by Bates *et al.* (1962), that the excited states can only be treated as quasi-steady state when the excited-state densities are much smaller than the ground-state density. Where inversions with respect to the ground state are not predicted (Figure 2.2(b)), the excited levels can be treated as quasi-steady state with reasonable accuracy.

2.3.2 Opacity considerations

The effect of a 90% self-absorption of L_α on the initial fractional ionization may be seen from Figure 2.1.

For example, for a carbon plasma at $N_e = 10^{21}$ cm^{-3} the fractional ionization increases by no more than a factor of two at the temperatures of interest - a variation which has no significant effect on the present results. Similarly, a calculation in which the absorption of L_α is assumed to remain constant (at 90%) with time, even though this is inconsistent with the computed densities, shows such an absorption has no significant effect on the densities (Figure 2.3).

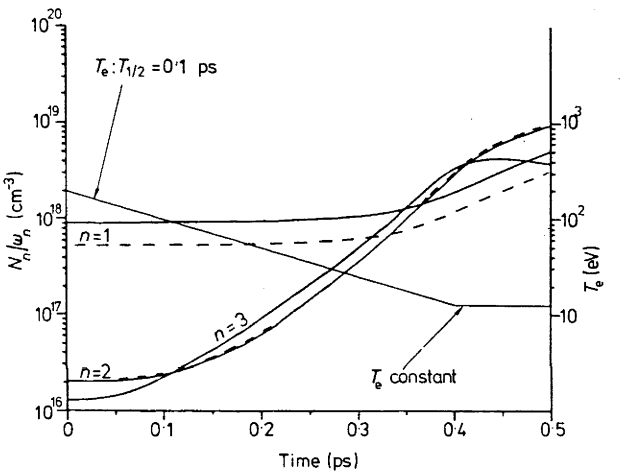

Figure 2.3: The time history of population densities N_n/ω_n (n = 1, 2 and 3) for a hydrogen-like carbon plasma which is initially in a steady state with $N_e = 10^{21}$ cm^{-3} and in which T_e decreases with time as shown, while N_e remains constant. The full curves correspond to an optically thin plasma, while the broken curves (included for comparison) correspond to a 90% self-absorption of L_α, assumed constant with time.

2.3.3 Initial temperature

At first sight a very high initial temperature appears to be desirable when trying to achieve population

inversions with respect to the ground state, since (see Figure 2.1) the proportion of electrons initially in the ground state is correspondingly low. However, at very high temperatures the number of electrons in the excited states is also low, and in effect we simply have to wait longer for the temperature to drop to a value ($Z^{-2}T_e$ < 3 eV) where inversions with respect to the ground state occur. This is illustrated in Figure 2.4 where the inversions occur sooner and at higher densities when the initial temperature is

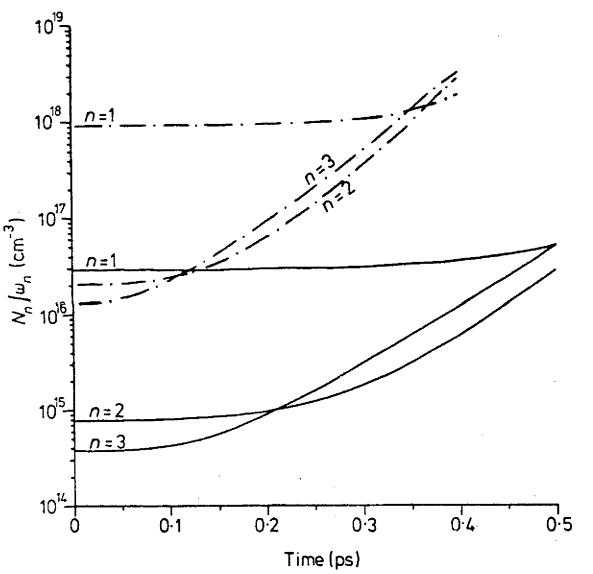

Figure 2.4: The time history of population densities N_n/ω_n (n = 1, 2 and 3) for an optically thin hydrogen-like carbon plasma which is initially in a steady state with $N_e = 10^{21}$ cm^{-3} and where T_e, initially equal to 2000 eV (full curves) or 200 eV (chain curves), subsequently decreases exponentially with a half-life of 0.1 ps while N_e remains constant.

200 eV compared to 2000 eV. The initial temperature must, however, be greater than the threshold for production of

fully stripped ions (i.e. greater than about 80 eV for carbon with $N_e = 10^{21}$ cm^{-3}). An initial temperature of 200 eV is appropriate for carbon, and we have used 200 eV as an initial temperature for most computations given in this paper.

2.3.4 Electron density and Z scaling

Figure 2.5 shows the maximum values of $T_{1/2}$ at which a $2 \rightarrow 1$ population inversion is predicted in hydrogen-like carbon plasmas cooling exponentially from 200 eV down to 12.5 eV (T_e = 12.5 eV represents four $T_{1/2}$ cycles from 200 eV). When cooling to a temperature less than 12.5 eV, $2 \rightarrow 1$ inversions can occur with slightly longer $T_{1/2}$ values.

From Figure 2.5 we see smaller values of $T_{1/2}$ are needed at higher electron densities, a trend which is a consequence of the relaxation times (McWhirter and Hearn 1963) becoming smaller with increasing electron density.

The results in Figure 2.5 (for carbon) do not scale strictly with atomic number. However, we have verified numerically that the Z scaling indicated in Figure 2.5 for $T_{1/2}$ is satisfactory. The scaling of the inversion densities $(N_2 - N_1\omega_2/\omega_1)$ is approximately proportional to Z^{10}.

Inversions with respect to the ground state are only produced at high electron densities ($Z^{-7}N_e > 10^{15}$ cm^{-3}, see Figure 2.5) and not-too-high electron temperatures

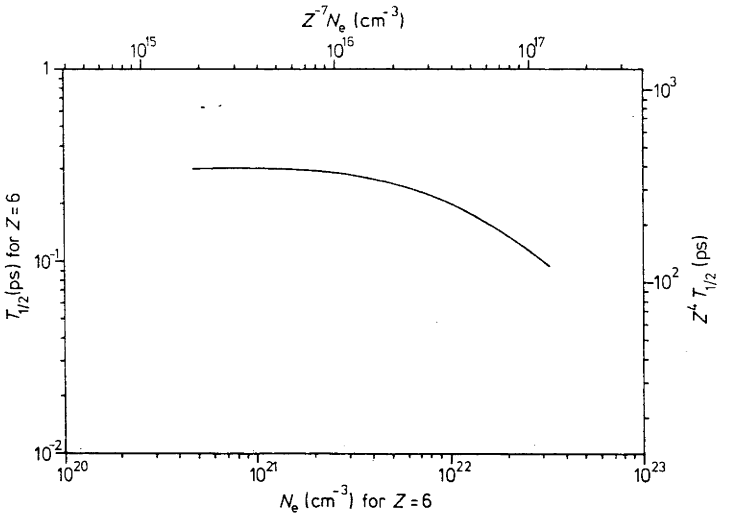

Figure 2.5: Plot showing the maximum value of $T_{1/2}$ as a function of N_e at which a population inversion between states $n = 2 \rightarrow 1$ is produced in an optically thin hydrogen-like carbon plasma initially in a steady state with T_e = 200 eV, and which subsequently cools down to T_e = 12.5 eV. The results scale with Z as indicated on the right-hand and top coordinate scales, with the initial electron temperature scaling as $(200/36)Z^2$ eV, and the final electron temperature as $(12.5/36)Z^2$ eV.

($Z^{-2}T_e \lesssim 3$ eV) where collisional processes dominate radiative processes in populating the ground and excited states. Assuming that we start with $Z^{-7}N_e$ close to 10^{15} cm^{-3}, this eliminates adiabatic expansion ($T_e^3 N_e^{-2}$ = constant) as a means of achieving population inversions with respect to the ground state. It also contrasts with the fact that predicted quasi-steady-state inversions between excited states (e.g. Bohn 1974, and see Chapter 3) occur only at electron densities $Z^{-7}N_e < 10^{15}$ cm^{-3} (the inversions calculated in this chapter

are produced by collisional processes, while those calculated in Chapter 3 are produced by radiative processes).

The results in Figure 2.5 correspond to $N_e \lesssim 3 \times 10^{22}$ cm^{-3}. For $N_e \gtrsim 3 \times 10^{22}$ cm^{-3} ($T_e \lesssim 12.5$ eV) the ionization potential for hydrogen-like carbon is smaller than the energy of the first excited state (see Marr 1968), and so for C^{5+} the first excited state cannot be regarded as discrete.

2.3.5 Plasma gain

It is of interest to calculate the gain coefficients for the population inversions indicated in Figure 2.3. The small signal gain $G(n,m)(cm^{-1})$ at the centre of a transition $n \rightarrow m$ is equal to

$$G(n,m) = \frac{\lambda^2}{4\pi} \frac{A(n,m)}{\Delta\nu} (N_n - \frac{\omega_n}{\omega_m} N_m) E \qquad (2.2)$$

where λ (cm) is the wavelength of the transition $n \rightarrow m$, $\Delta\nu$ (s^{-1}) is the full half-width of the transition, and E is a constant which depends on the shape of the line profile. For example, E takes values of $(\ln 2/\pi)^{1/2} = 0.47$ for a Gaussian profile, $1/\pi = 0.32$ for a Lorentzian profile and $[5/(4\pi)]\sin(2\pi/5) = 0.38$ for the profile $1/\{1 + [2(\nu - \nu_0)/\Delta\nu]^{5/2}\}$ which approximates an ion quasi-static Stark-broadened line profile (Irons 1977 private communication).

TABLE 2.1

Gain coefficients for C VI transitions (n,m) using the data from Figure 2.3 (optically thin case)

Time (ps)	G(2,1) (cm^{-1})	G(3,2) (cm^{-1})	G(3,1) (cm^{-1})
0.10			
0.15		7.6^{-1}	
0.20		2.4	
0.25		5.6	
0.30		1.2^{1}	
0.35		3.0^{1}	1.8^{-2}
0.40	3.0^{1}*	3.3^{1}	1.5
0.45	7.2^{1}		1.8
0.50	9.4^{1}		

* Read 3.0^{1} as 3.0×10^{1}

Wavelengths and halfwidths of the transitions:

$\lambda(2,1) = 33.8$ Å $\quad \Delta\nu(2,1) = 6.94^{14}$ s^{-1}

$\lambda(3,2) = 182.3$ Å $\quad \Delta\nu(3,2) = 1.16^{15}$ s^{-1}

$\lambda(3,1) = 28.5$ Å $\quad \Delta\nu(3,1) = 1.85^{15}$ s^{-1}

At electron densities $N_e \simeq 10^{21}$ cm^{-3} and temperatures $T_e \simeq 200$ eV, ion quasi-static Stark broadening dominates electron impact Stark broadening and thermal Doppler broadening for the lines of interest here (substitute into equations (4) and (5) of Irons (1973)), and so halfwidths $\Delta\nu$ may be calculated from the ion quasi-static formula (equation (4) of Irons (1973) with $(n_\ell + \frac{1}{2})$ replaced by $\frac{1}{2}(n_u^2 - n_\ell^2)$; see also Griem (1974)). The ion quasi-static halfwidths appropriate to Figure 2.3 are listed below

Table 2.1, and setting $E = 0.38$ have been used to calculate the values of G listed in Table 2.1.

G(2,1) and G(3,2) in Table 2.1 are sufficiently large that amplification can occur over distances found in laser-produced plasmas (e.g. 100 μm). However, the evaluation of net gain in a differentially expanding plasma, such as a laser-produced plasma is rather more complex than is suggested by equation (2.2) (see Irons (1976) for a detailed discussion).

2.4 Plasma Cooling Rates

2.4.1 MEDUSA results

The one-dimensional numerical code MEDUSA (Christiansen *et al.* 1974) with the version 2A corrections (Christiansen *et al.* 1975) was used to indicate how, in practice, T_e might decrease with time. A sphere of fully ionized plasma at a uniform initial temperature and density was considered to expand freely. The MEDUSA calculations presented here consider only plasma expansion such as in a laser-produced plasma after the laser light is extinct: the code was not used to simulate the effect of an incoming laser pulse.

MEDUSA predicts that at the centre of an initially uniform expanding plasma sphere, T_e decreases approximately exponentially, while N_e remains approximately constant (see,

TABLE 2.2

MEDUSA results for T_e, $T_{1/2}$ and N_e as a function of time at the centre of a freely expanding carbon plasma sphere of initial radius 0.1 μm

Time (ps)	T_e (eV)	$T_{1/2}$ (ps)	N_e (10^{21} cm^{-1})
0.00	200		1.0
0.33	100	0.33	0.99
0.68	50	0.35	0.97
1.11	25	0.42	0.89
1.64	12.5	0.53	0.68

for example, the results of Table 2.2). Physically, the boundary region of the plasma expands and cools, and the central region is cooled primarily by thermal conduction to the boundary. Without going into the details of MEDUSA (this is done in Christiansen *et al.* 1974), we mention that the MEDUSA electron thermal conduction flux (F_e^l) is limited to the free-streaming value according to

$$\frac{1}{F_e^l} = \frac{1}{F_e} + \frac{1}{(F_e)_{max}} \qquad (2.3)$$

where $(F_e)_{max}$ is the free-streaming flux, and F_e is the flux assuming many mean free paths for thermal conduction.

Using the MEDUSA code we found $T_{1/2}$ for a plasma sphere is approximately $\frac{2}{3}$ x $T_{1/2}$ for a plasma cylinder, and approximately $\frac{1}{3}$ x $T_{1/2}$ for a plane-parallel plasma slab (where the sphere radius = cylinder radius = slab thickness).

2.4.2 A simple model

Some of the MEDUSA results of Section 2.4.1 can be approximated using the following simple model for the cooling at the centre of an expanding plasma. We assume $T_{1/2}$ at the centre of a plasma is given by the time for a "cold" rarefaction wave travelling at the ion acoustic speed v_s(cm s^{-1}) to travel from the edge of the plasma to the centre, i.e.

$$T_{1/2} = r_0/v_s \tag{2.4}$$

where r_0 (cm) is the initial radius of the plasma. For the ion acoustic speed v_s we have

$$v_s = 9.79 \times 10^5 \left(\frac{T_i + ZT_e}{M}\right)^{1/2} \tag{2.5}$$

where T_i (eV) is the ion temperature and M the atomic weight of the plasma. Setting $T_e = T_i$ to the initial temperature of the plasma T (eV)

$$T_{1/2} = 10^{-6} r_0 \left(\frac{M}{T(Z + 1)}\right)^{1/2} \tag{2.6}$$

Values of $T_{1/2}$ from this equation for carbon (Z = 6, M = 12) presented here in Figure 2.6 are seen to be comparable to MEDUSA $T_{1/2}$ values (also shown in Figure 2.6).

The MEDUSA results of Figure 2.6 and $T_{1/2}$ results of equation (2.6) do not change greatly when calculated for

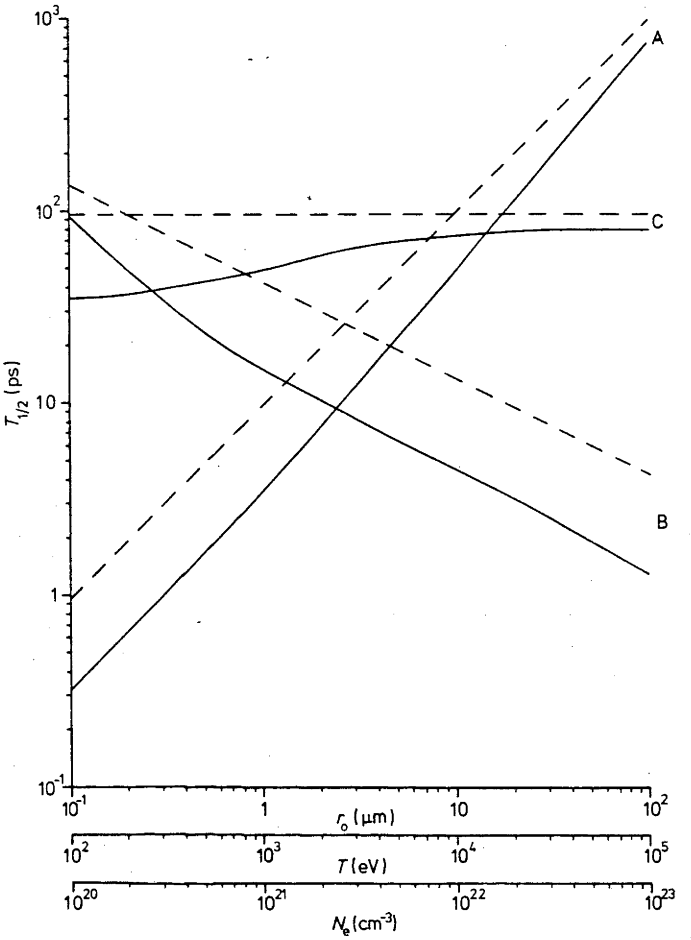

Figure 2.6: Electron temperature half-life ($T_{1/2}$) at the centre of an expanding carbon plasma sphere: full curves, from MEDUSA results; broken curves, from equation (2.6). The half-life is plotted (A) as a function of the initial radius (r_0) of the sphere with initial temperature and density of T = 200 eV and $N_e = 10^{21}$ cm^{-3}, (B) as a function of initial T with initial r_0 = 10 μm and initial $N_e = 10^{21}$ cm^{-3}, and (C) as a function of initial N_e with initial r_0 = 10 μm and initial T = 200 eV.

elements other than carbon. This can be explained by referring to equation (2.6) where $T_{1/2}$ scales with $[M/(Z+1)]^{1/2}$ - the ratio $[M/(Z+1)]^{1/2}$ only varies from 1.16 for He to, e.g. 1.44 for Fe.

2.4.3 Laser-produced plasmas

Very small plasmas seem necessary (Figure 2.6) to achieve the small $T_{1/2}$ values required (Figure 2.5) for the production of population inversions with respect to the ground state for hydrogen-like ions. Spherical carbon plasmas of radius less than about 0.1 μm can (according to Figures 2.5 and 2.6) cool rapidly enough upon free expansion to produce such inversions. Cylindrical carbon plasmas of radius less than about 0.07 μm can also cool fast enough to produce the inversions (a plasma sphere cools approximately 50% faster than a plasma cylinder, see Section 2.4.1). Also with a cylindrical plasma, amplified spontaneous emission (ASE) can occur preferentially along the cylinder axis (to observe superradiance a cylinder of length about 100 μm would be needed, see Section 2.3.5).

The small plasmas necessary to produce hydrogen-like ion inversions with respect to the ground state may be created perhaps by laser-driven compression (e.g. Nuckolls *et al.* 1972, Hora 1976), though the compression requirements to produce, for example, the cylindrical plasma needed for ASE mentioned above are formidable and certainly beyond the present-day capability. In the absence of compression, laser-produced plasmas appear inherently to be too large for inversions to occur (see e.g. Salzmann (1973) where the thickness of various laser-produced plasmas have been deduced experimentally). Short laser cut-off times of the order of

the required $T_{1/2}$ values are also probably necessary (e.g. around 10^{-13} s for C VI inversions with respect to the ground state). With laser-driven compression, short laser cut-off times are probably not needed because the inertia of the compression process should ensure that compression continues as the laser cuts off.

Another way to create a small plasma is to use self-focusing of laser radiation. There is theoretical evidence that "hot" (∿200 eV) thin (∿wavelength of the laser) plasma filaments can be produced in a "cold" (∿10 eV) plasma by self-focusing of laser radiation (e.g. Hora 1975, Siegrist 1976). For C VI 2 → 1 (33.8 Å) inversions, however, we require plasma filaments of radius less than about 0.1 μm, and hence a laser of similar wavelength ($\lambda \leq 0.1$ μm = 1000 Å).

2.5 Scaling with Atomic Number

So far we have primarily treated inversions in hydrogen-like carbon ($Z = 6$), but as indicated in Section 2.3.4, if we scale the initial T_e as Z^2, then the minimum N_e at which inversion occurs scales as Z^7, the required $T_{1/2}$ for inversion as Z^{-4}, and the inversion density $(N_n - N_m\omega_n/\omega_m)$ as approximately Z^{10}. With this scaling the full half-linewidth (assuming either ion quasi-static or electron impact Stark broadening) varies as $\Delta\nu \propto Z^4$, and the gain coefficient as $G \propto Z^6$. In Section 2.4.2 we also showed that the cooling rates for plasmas of given initial

r_0 and T are largely independent of the plasma ion Z (provided the ions are close to fully stripped). With the $T_{1/2}$ and T_e scaling indicated above, from equation (2.6) we thus have the required initial radius r_0 for a plasma to cool sufficiently fast to produce inversions with respect to the ground scaling as $r_0 \propto Z^{-3}$.

Table 2.3, obtained using the above scaling rules, shows for different Z the values of various parameters associated with hydrogen-like ion inversions with respect to the ground state. The gain coefficients are calculated assuming quasi-static Stark broadening, which for all Z under the conditions specified in Table 2.3 dominates thermal Doppler broadening and electron impact Stark broadening (see the formulae in Irons (1973)).

Table 2.3 clearly indicates that ASE due to hydrogen-like ion inversions with respect to the ground state will be difficult to produce experimentally. For example, to observe ASE at 304 Å for Z = 2, we require an initial cylindrical plasma of length $\sim$10 cm and radius $\simeq$2 μm. The necessary conditions for higher Z inversions are even more difficult to produce.

2.6 Conclusion

Population densities of excited and ground states of hydrogen-like ions have been computed on a time-dependent

TABLE 2.3

The variation with atomic number of parameters associated with inversion with respect to the ground state in hydrogen-like ions

Z	$\lambda(2,1)$ (Å)	$T_{1/2}$ (s)	Initial T_e (eV)	Initial N_e (cm^{-3})	Initial r_0 (μm)	G(2,1) (cm^{-1})
2	304	2^{-11}*	20	5^{17}	3	1^{-1}
3	135	5^{-12}	50	8^{18}	0.8	2
4	76	2^{-12}	90	6^{19}	0.3	9
5	49	6^{-13}	140	3^{20}	0.2	3^{1}
6	34	3^{-13}	200	1^{21}	0.1	1^{2}
7	25	2^{-13}	270	3^{21}	0.06	3^{2}
8	19	1^{-13}	360	7^{21}	0.04	6^{2}

* Read 2^{-11} as 2×10^{-11}

basis for an initially steady-state plasma in which the electron temperature subsequently decays exponentially with a half-life $T_{1/2}$. Computations for Z = 6 (carbon) at an initial temperature T_e = 200 eV and electron density $N_e = 10^{21}$ cm^{-3} indicate that, to achieve inversions with respect to the ground state, $T_{1/2}$ must be smaller than about 3×10^{-13} s. Further computations show that the values of $T_{1/2}$ necessary to achieve inversions with respect to the ground state are consistent with "radial" plasma dimensions less than approximately 0.1 μm. Possible methods of creating

laser-produced plasmas of such small size are discussed (Section 2.4.3). An indication is given (Section 2.5) of the scaling with atomic number of the parameters associated with hydrogen-like ion inversions with respect to the ground state.

CHAPTER 3

THE EFFECT ON LYMAN α SELF-ABSORPTION ON POPULATION INVERSIONS BETWEEN QUANTUM STATES 2 AND 3

3.1 Introduction

Self-absorption of resonance radiation can prevent the development of population inversions between excited quantum states of hydrogen-like ions (see e.g. Irons and Peacock 1974). In this chapter we extend the treatment by Bohn (1974) of quasi-steady state inversions between excited states of hydrogen-like ions under optically thin conditions, to include Lyman α self-absorption. Following Bohn (1974) we treat the electron density and temperature as independent variables, and deduce density-temperature regimes where $3 \rightarrow 2$ inversions occur. Bohn has suggested that the density-temperature regimes predicted as giving rise to inversions can be encountered in plasma dynamic expansions. The present work has been motivated by our interest in one such plasma dynamic expansion, namely the expansion plume of the laser-produced plasma.

3.2 Calculations

We use the usual reduced parameters, namely (McWhirter and Hearn 1963):

Electron temperature $\theta = T_e/Z^2$ (°K)

Electron density	$\eta_e = N_e/Z^7 \quad (cm^{-3})$
Population density of quantum state n	$\eta_n = N_n X/Z^{11} (cm^{-3})$

where Z is the ion atomic number, and X is the ratio of the electron density (N_e) to the fully stripped ion density.

It is unnecessary to assign an absolute value to X as we are only interested in relative excited state densities, these being sufficient to determine when an inversion between excited states exists. We regard Θ, η_e and η_1 as independent variables. The (relative) values of η_n ($n > 1$) have been computed assuming the quasi-steady state approximation and using the computer code COLLRAD (see Appendix A). For the COLLRAD calculations we have used the rate coefficients cited or tabulated by McWhirter and Hearn (1963). From the computations, regimes have been identified (Figures 3.1 and 3.2) where population inversions between quantum states n = 2 and 3 occur.

As it enters into rate equations describing population density, photo-excitation may be represented as a reduction in the spontaneous emission coefficient A(n, m) (for a transition from state n to m) to a value A(n, m) Λ(n, m). The coefficient Λ(n, m) is related in a complex way (via the equation of radiative transfer) to the plasma parameters. In laser-produced plasmas, in particular, we note that because of the complex, time-dependent geometry, as well as the gross plasma inhomogeneity and the presence

of ion streaming (e.g. Irons *et al.* 1972), it is virtually impossible to calculate values of Λ with any precision. Consequently, we follow the example of those authors who study the influence of photo-excitation arising from self-absorption by assigning numerical values to Λ (e.g. Drawin 1969, 1970; Drawin and Emard 1970; Bohn 1971; Drawin *et al.* 1973; Skorupski and Suckewer 1974).

However, some guidance as to the approximate values of Λ appropriate to the expansion plume of laser-produced plasmas can be given, and to this end we proceed as follows (F.E. Irons private communications). Firstly, we neglect the effect of ion streaming. An estimate of Λ is then provided by the probability T that a Lyman α photon propagates an optical depth τ characteristic of the shortest dimension of the laser-produced plasma and escapes. Close to the target surface, the broadening of a hydrogen-like line such as CVI L_α is predominantly ion quasi-static, and $\tau \simeq 70$ at a distance 300 μm from the target when we take typical (e.g. Galanti and Peacock 1974) parameters $N_e = 10^{20}$ cm^{-3} and $N_1 = 10^{19}$ cm^{-3}. This gives $T \simeq 0.05$, and hence, as a first approximation, $\Lambda(2, 1) \simeq 0.05$ at 300 μm from the target. The presence of ion streaming increases the probability of photon escape (e.g. Irons 1975, 1976), and with increasing distance from the target, as the plasma density decreases and ion streaming becomes the dominant cause of broadening, so $\Lambda(2, 1)$ approaches unity (the optically thin value). Consequently, for this chapter it is appropriate

to choose values of $\Lambda(2, 1)$ in the range 0.05 - 1.0. In fact our calculations (see Figures 3.1 and 3.2) indicate that values of $\Lambda(2, 1) \lesssim 0.4$ inhibit the development of $3 \rightarrow 2$ population inversions, and so our interest is restricted to values $\Lambda(2, 1) \gtrsim 0.4$. For values of $\Lambda(2, 1) \gtrsim 0.4$, we may set Λ values for all other transitions (including other resonance transitions) to unity (see e.g. Drawin 1970).

3.3 Discussion

Population inversions between excited states of hydrogen-like ions in recombining plasmas are produced because, with decreasing principal quantum number, radiative de-excitation (a process not generally balanced by the inverse photo-excitation) becomes more important than collisional de-excitation, and population densities depart progressively further below their Saha-Boltzmann values. A useful concept in this respect is the thermal limit, which, following McWhirter (1965) we define as the lowest quantum state for which the rate of collisional de-excitation into the neighbouring lower state exceeds the corresponding radiative rate by a factor-of-ten. A quantum state n is thus greater than the thermal limit provided (equation (10) of McWhirter (1965), expressed in reduced parameters).

$$\eta_e > 1.6 \times 10^{12}\, \theta^{\frac{1}{2}} [\chi(n, n-1)]^3 \qquad (3.1)$$

where $\chi(n, m) = 13.6\ (n^2 - m^2)/(n^2 m^2)$ is the reduced energy

separation of states n and m in electron volts. For example, quantum states n = 3, 4 and 5 are above the thermal limit provided $\eta_e > 1 \times 10^{15}$ cm^{-3}, $\eta_e > 4 \times 10^{13}$ cm^{-3}, and $\eta_e > 4 \times 10^{12}$ cm^{-3} respectively, for $\Theta = 8000°K$ (though the dependence on Θ is comparatively small).

The computations of Bohn (1974), as well as the present computations (Figure 3.1), show that inversions between quantum states n = 2 and 3 in hydrogen-like ions are only possible for $\eta_e < 10^{15}$ cm^{-3}. We note that this is just the condition for the state n = 3 to be <u>below</u> the thermal limit; a condition which provides an insight into the balance between collisional and radiative de-excitation needed to produce inversions between excited quantum states (see the definition of the thermal limit, equation (3.1)).

Bohn (1974) was concerned with plasmas not too far removed from equilibrium, so that collisional excitation from the ground state influenced excited state densities (primarily η_2) and acted to upset 3 → 2 conversions. The maximum value of η_1 (denoted by η_1^{max}) which can be tolerated and still achieve an inversion is plotted in Figure 3.1 for $\Theta = 8000°K$ as a function of η_e (the optically-thin curve is identical to that of Bohn 1974). With decreasing η_e, the excited state densities decrease rapidly in magnitude (as η_e^2 for states above the thermal limit), and η_1^{max} correspondingly decreases.

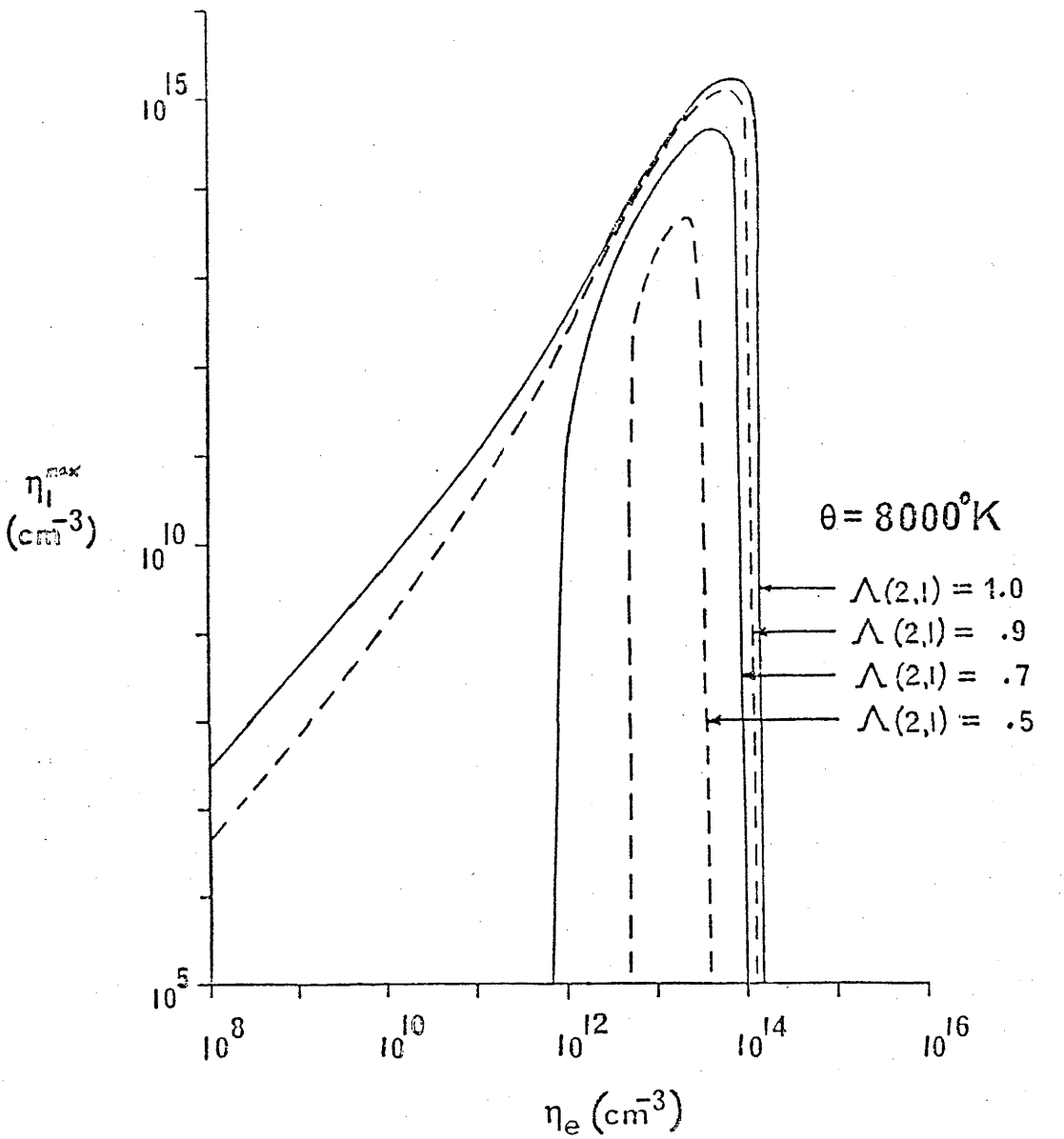

Figure 3.1: The maximum reduced ground state density η_1^{max} for an inversion to occur between quantum states n = 2 and 3 at a reduced electron temperature Θ = 8000°K, plotted as a function of reduced electron density η_e for various values of $\Lambda(2, 1)$ (as indicated). All $\Lambda(n, m)$ other than $\Lambda(2, 1)$ are set equal to unity.

When Lyman α self-absorption is included (Figure 3.1) η_1^{max} decreases for a given η_e because the increased excitation from the ground state (now photo-excitation as well as collisional excitation) has a correspondingly greater effect on η_2. Indeed inversions may become impossible for small η_e, where spontaneous emission is the dominant de-excitation mechanism from state n = 2 and where self-absorption is correspondingly more effective in influencing η_2. We note that the computations of Bohn (1971), on the effect of self-absorption of all Lyman lines on the inversion 5 → 3 in hydrogen atoms, show a similar trend to that in Figure 3.1.

We are interested in laser-produced plasmas, which are usually far from equilibrium (i.e. $\eta_1 << \eta_1^{max}$), so we choose to present our principal results as in Figure 3.2. This figure, assuming $\eta_1 << \eta_1^{max}$, shows the maximum Lyman α self-absorption (i.e. the smallest value of $\Lambda(2, 1)$) which can be tolerated and still achieve a 3 → 2 inversion, plotted as a function of η_e for several values of Θ. The curves show minima at electron densities η_e in the range 10^{13} to 2×10^{13} cm^{-3} where the thermal limit is just above quantum state n = 4. At high electron densities, where the thermal limit is below quantum state n = 3, population inversions do not occur even in the optically-thin case. At low electron densities, only a small amount of self-absorption can be tolerated (as discussed above).

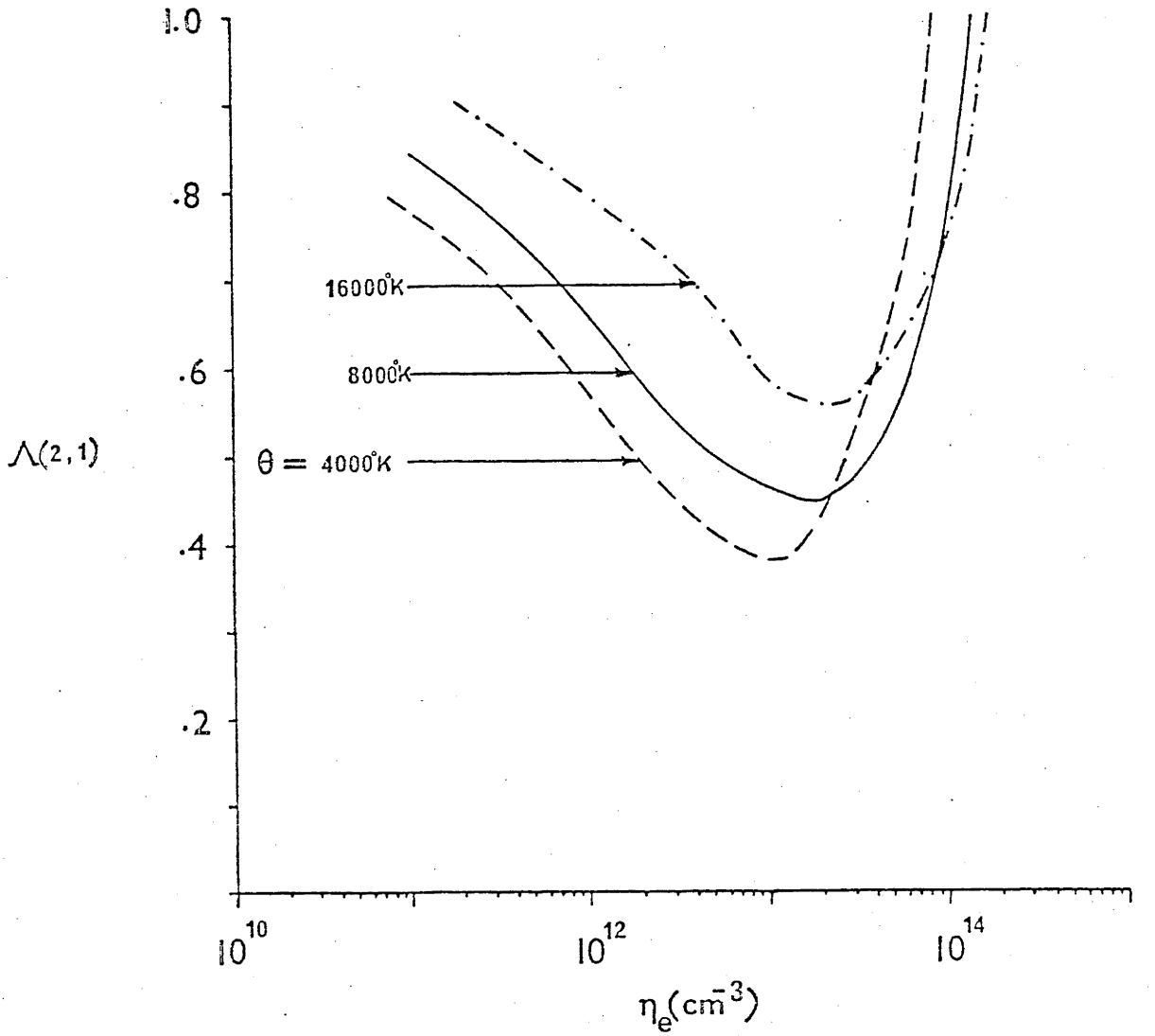

Figure 3.2: The minimum value of $\Lambda(2, 1)$ for which $3 \rightarrow 2$ population inversions occur, plotted as a function of reduced electron density η_e for various reduced electron temperatures Θ. All $\Lambda(n, m)$ other than $\Lambda(2, 1)$ are set equal to unity. Collisional excitation from the ground state is assumed to be negligible - that is we assume $\eta_1 << \eta_1^{max}$.

3.4 Plasma Cooling Rates

In Chapter 2 we calculated the electron cooling rates required to achieve population inversions with respect to the ground state in hydrogen-like ions. Rapid cooling was found necessary, with eg for carbon, temperature half-lives $T_{1/2} \lesssim 3 \times 10^{-13}$ second (the decisive relaxation time for inversions with respect to the ground state is that of the upper quantum state involved in the transition). The required cooling rates for inversions between excited quantum states, however, are much smaller (as here the decisive relaxation time is that of the ground quantum state). A $T_{1/2}$ value somewhat smaller than the ground state relaxation time (as tabulated in eg Drawin 1970) will be sufficient to result in $\eta_1 < \eta_1^{max}$, and hence the possibility of a $3 \rightarrow 2$ inversion (if L_α self-absorption is not too great). For example, with $\eta_e = 10^{14}$ cm^{-3}, $\Theta = 16\,000$ °K we require $T_{1/2} < Z^{-4} \times 1.2$ seconds (!), a value readily achieved in a laser-produced plasma.

3.5 Conclusion

We have computed the effect of Lyman α self-absorption on quasi-steady state population inversions between quantum states n = 2 and 3 of hydrogen-like ions. The range of electron densities over which population inversion is possible has been shown to diminish when Lyman α self-absorption increases. The highest degree of absorption which can be tolerated and still achieve an inversion

occurs when the thermal limit corresponds to $n \approx 4$. The computations have been related to conditions in the expansion plume of a laser-produced carbon plasma.

PART II

CHAPTER 4

THE OPERATION OF A 45° PARALLEL PLATE ELECTROSTATIC ANALYZER IN LASER-PRODUCED PLASMA STUDIES

4.1 Introduction

In this chapter we describe the laser (Section 4.2), the laser-produced plasma (Section 4.3), and the electrostatic ion energy analyzer (Section 4.4). In Chapter 5 we examine space charge effects within the analyzer. The principal results (ion energy spectra) are presented and discussed in Chapter 6.

4.2 The Laser

The laser layout is illustrated in Figure 4.1. The Nd:Yag oscillator produces a Q-switched TEM_{00} pulse of 50 mJ of 8 ns FWHM. The pockels cell PC1 is triggered when the oscillator fires via a spark gap, and switches on (allowing light to pass) for 4 ns. The other pockels cell PC2 is driven from the same transmission line as PC1, and similarly opens for 4 ns. PC2 acts as an optical isolator to (i) improve the contrast ratio of the 4 ns pulse, (ii) prevent amplified spontaneous emission in the amplifiers, and (iii) prevent back-reflected light reaching the early stages of the laser. The laser has four amplification

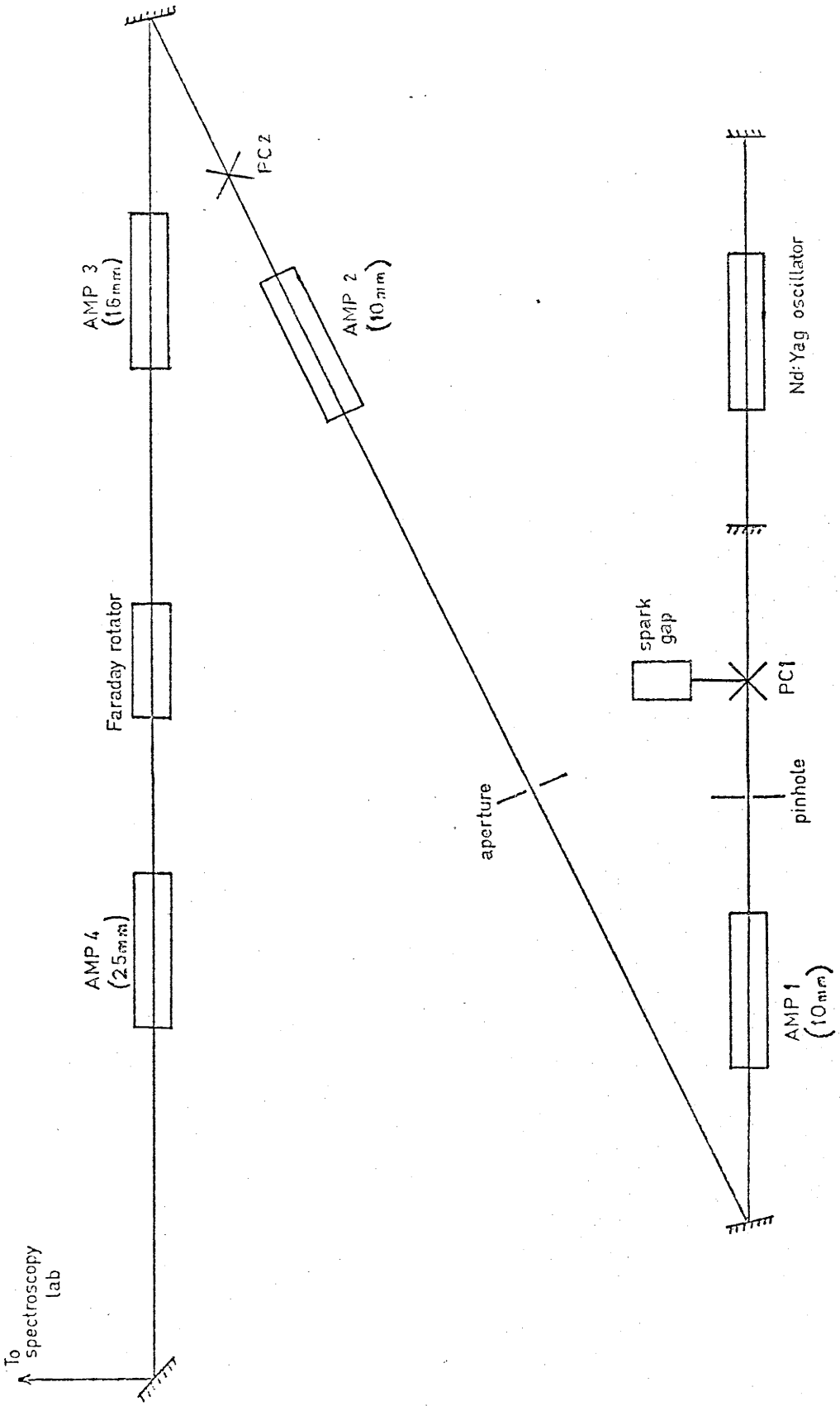

Figure 4.1: Schematic of the laser layout. The pinhole and aperture define the laser divergence and beam spatial distribution. The amplifier rod diameters are given in brackets.

stages of Nd doped glass rods pumped by flashlamps. A Faraday rotator (see Gillman 1977) provides additional protection against back-reflection.

Due to the switching-out actions of the pockels cells, the output laser pulse is approximately rectangular (see Figure 4.2), and of duration 4 ns. The output power is varied by adjusting the current through the amplifier flashlamps. For the present experiments we have operated so that the power (averaged over the pulse length) is in the range 190 to 810 MW.

4.3 The Laser-Produced Plasma

The laser-produced plasma is created by focusing the laser onto a plane carbon target. The experimental lay-out is illustrated in Figure 4.3. The target chamber pressure is typically ≈ 1 mPa. To focus the laser we use a CILAS lens doublet designed to minimise spherical aberration. The lens focal length and diameter are 100 mm and 50 mm respectively. The laser light reaches the lens through the window in the target vacuum chamber and strikes the target at about 20° to the surface normal. The lens was set 0.8 mm closer to the target than the distance of optimum focus (where back-reflection is at a maximum) in order to reduce the back-reflection and so reduce the possibility of damage to the laser. Using X-ray pinhole camera pictures and grazing incidence spectrograph space scans (obtained by F.E. Irons

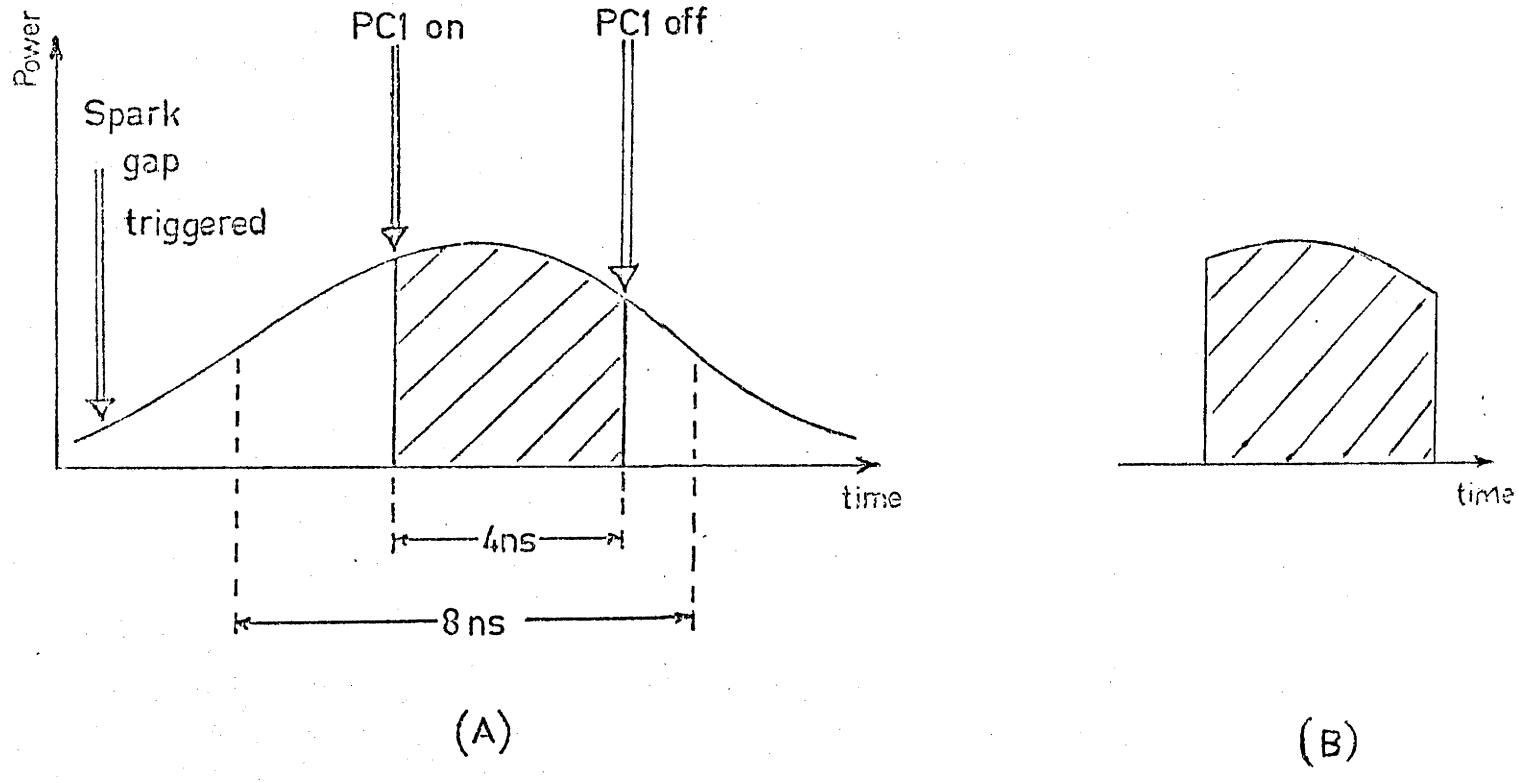

Figure 4.2: The laser pulse shape - (A) shows the oscillator output with the section selected by the Pockels cell PC1 hatched; (B) shows the resultant pulse.

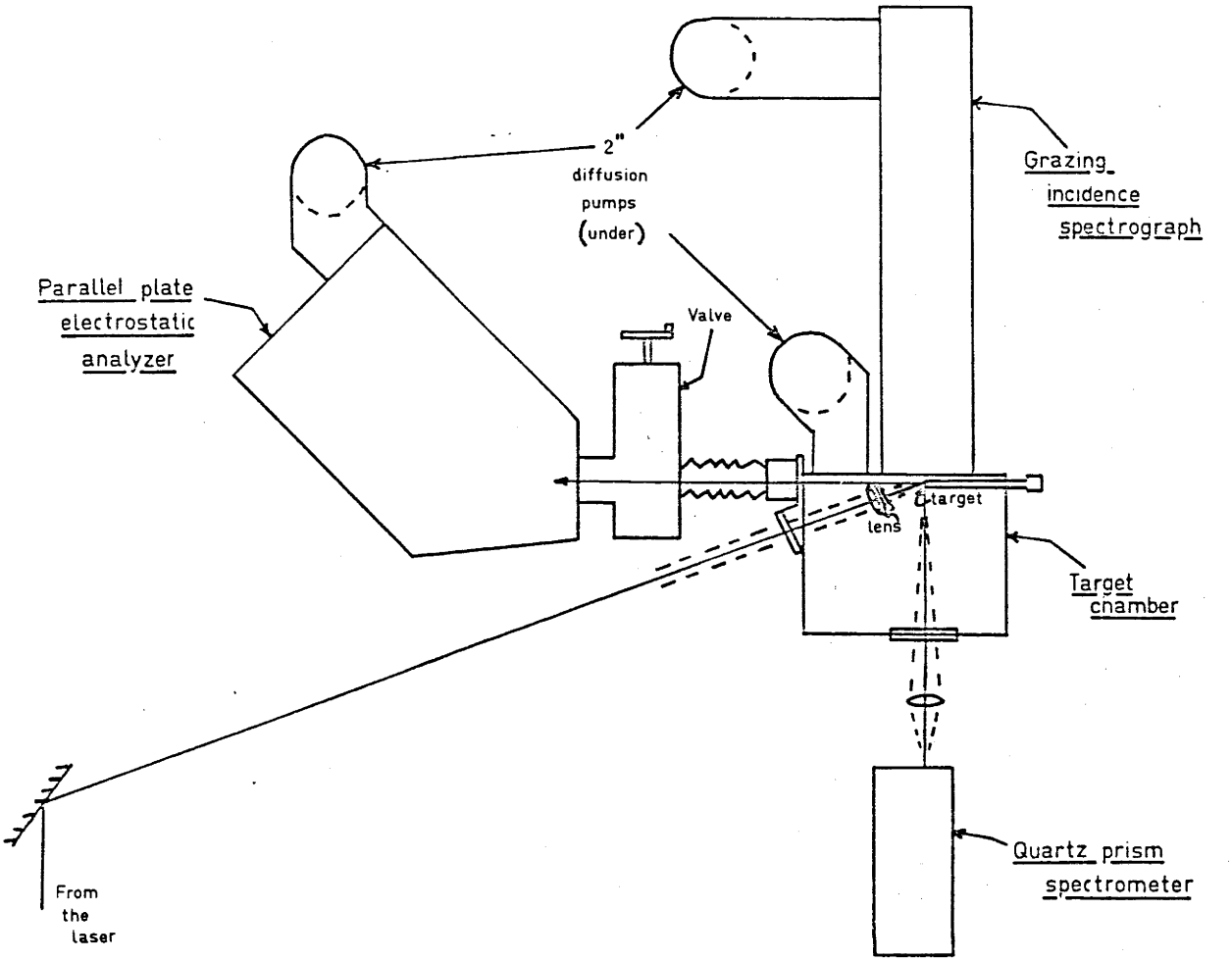

Figure 4.3: Schematic of the experiment.

and K.G. Renner of this laboratory), the focal spot diameter at the target surface was found to be ≈280 μm. This means we operate with laser flux intensities at the target surface in the range 3×10^{15} to 1.3×10^{16} Wm^{-2}.

4.4 The Parallel Plate Electrostatic Analyzer (PPEA)

The parallel plate electrostatic analyzer (hereafter referred to as the PPEA), first described by Yarnold and Bolton (1949) and Harrower (1955), has in recent years been discussed theoretically (Green and Proca 1970, Proca and Green 1970, Allen 1971), and used for the energy and mass analysis of ions from laser-produced plasmas (Oron and Paiss 1973, Charatis et al. 1974, Goforth 1975, 1976). We have constructed a 45° PPEA, as described below.

4.4.1 Description

The analyzer (illustrated in Figure 4.4) comprises two capacitor plates, namely the ground plate (at earth potential) and the deflecting plate (at a potential of up to + 12 kV), with four guard rings equispaced between the plates. The entrance slit in the ground plate is 800 mm from the target, and lies on a line through the point of laser impact normal to the target surface. The analyzer is inclined at 45° to the target normal, and is enclosed in a vacuum chamber pumped to ∿1 mPa which is coupled to the target chamber. Precautions were taken to ensure that ions

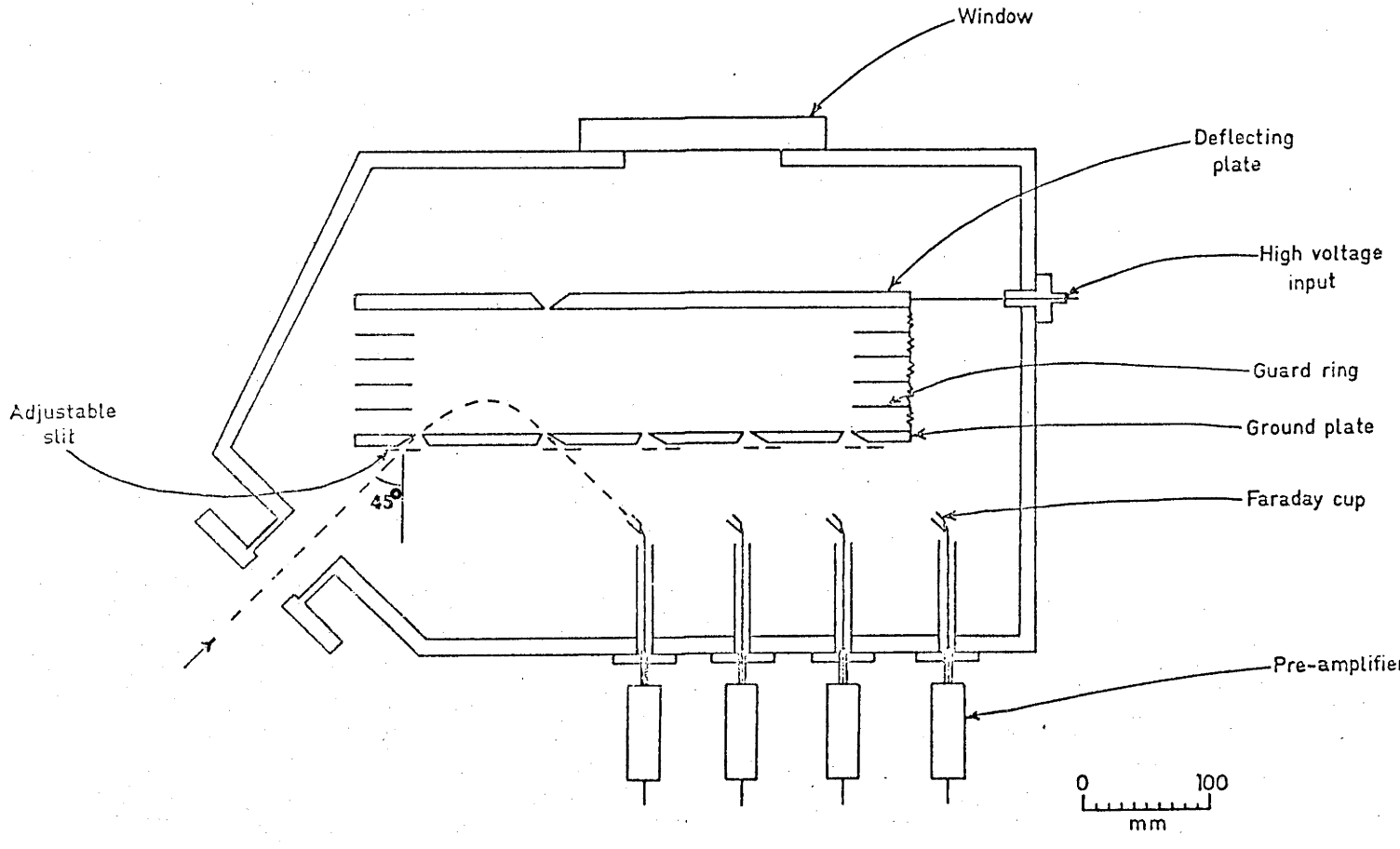

Figure 4.4: Diagram of the 45° parallel plate electrostatic analyzer described in Section 4.4.1 The exit apertures are on the ground plate at distances x = 100 mm (channel 1), 180 mm (channel 2), 260 mm (channel 3) and 340 mm (channel 4) from the entrance aperture. A possible ion trajectory is shown as a broken line.

reaching the entrance slit of the PPEA come directly from the plasma and are not scattered from the walls of the vacuum vessels.

First order focussing of the ions onto the inside surface of the ground plate occurs with an energy selection dependent on the distance x (mm) from the entrance slit such that

$$x = 2\ (E/Z)/(V/d) \tag{4.1}$$

where

E (eV) is the ion kinetic energy,

Z is the ion charge,

V (volts) is the deflecting plate potential, and

d (mm) is the distance between the deflecting and ground plates.

In the absence of space charge effects, the energy resolution $\Delta E/E$ is given by

$$\Delta E/E = (W_{ent} + W_{exit})/x \tag{4.2}$$

where W_{ent} (mm) is the entrance slit width, and W_{exit} (mm) the exit slit width.

We have incorporated adjustable entrance and exit slit widths in the analyzer (see Appendix B for a description of the slit mechanism). The adjustable slit jaws are slightly displaced from the plane of focus of the analyzer (the inside surface of the ground plate). This does not affect the

analyzer output signal provided we ensure that the divergence of the ion beam entering the analyzer is smaller than the sum of the angles subtended by the adjustable entrance and exit slit widths at the inside surface of the ground plate. For the beam divergence in our experiment ($\sim$5 mrad), this criterion is satisfied provided the sum of the entrance and exit slit widths exceeds 0.1 mm; a condition which is always satisfied in this experiment.

The ion detectors in the analyzer are deep Faraday cups. Each cup is connected by a coaxial cable to a fast (100 MHz) preamplifier of current gain x 1000, the output signal from which (across a 50Ω load) is displayed on a Tektronix 475 oscilloscope.

4.4.2 Operation

The PPEA combines energy selection with time-of-flight velocity selection. Ions of the same E/Z are recorded by the same Faraday cup, but because of the time-of-flight separation, the different Z ions are separated in their arrival time. Examples of Faraday cup outputs are shown in Figure 4.5. The width of each current pulse arises mainly from the finite time duration over which the ions are emitted.

Energy and velocity spectra have been built up on a shot-to-shot basis by varying the voltage V on the deflecting plate of the analyzer. The energy density N(E) ($keV^{-1}s^{-1}$)

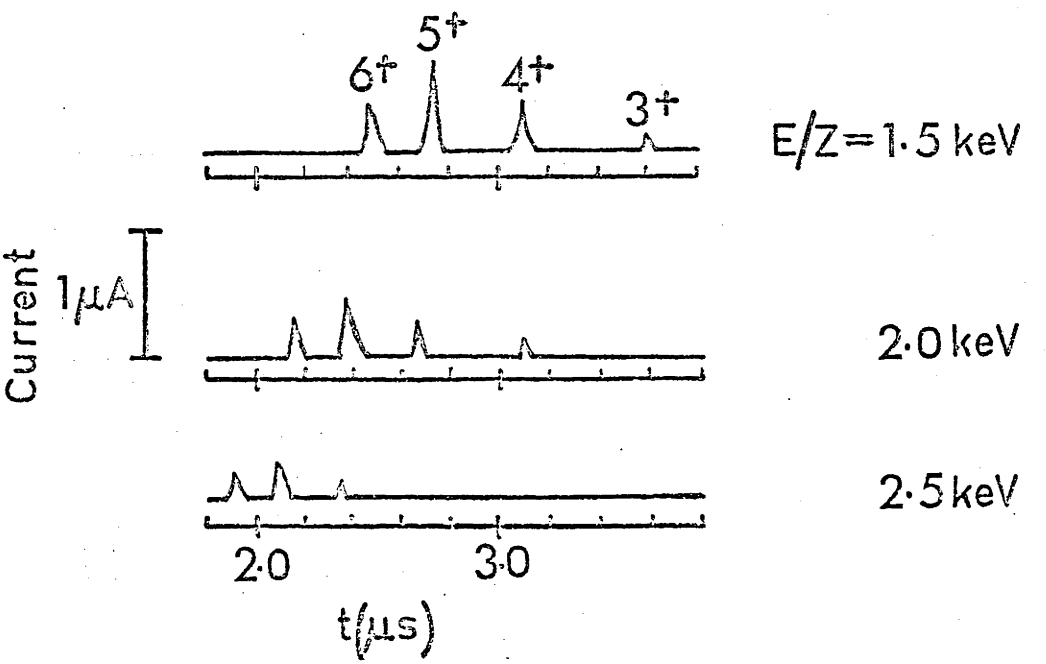

Figure 4.5: The PPEA channel 1 detector output for E/Z = 1.5 keV, 2.0 keV and 2.5 keV as indicated. Current peaks corresponding to C^{6+}, C^{5+}, C^{4+} and C^{3+} can be seen. The oscilloscope is triggered 1.8 μs after the laser pulse and the time divisions are 0.2 μs. The entrance slit width W_{ent} = 0.1 mm, and the laser intensity on target is 10^{16} W m^{-2}.

of ions entering the PPEA entrance slit is obtained using the relationship $N(E) = I/[(Ze)\Delta E]$, where I (amps) is the peak current signal measured for ions in the energy range $E \pm \Delta E/2$. Using equation (4.2) we have

$$N(E) = \frac{I}{(Ze)E} \frac{x}{W_{ent} + W_{exit}} \qquad (4.3)$$

Examples of energy spectra are presented in Chapter 6 (see Figures 6.1 to 6.4).

We have investigated the effect of the analyzer background gas pressure on the PPEA response by recording spectra at different pressures. Variations in the spectra in excess of experimental errors were not detected over 1-10 mPa, but at 15 mPa we found the number of ions measured to be somewhat reduced, though the energy where the spectra N(E) peak, remained the same. Operation at $\simeq$1 mPa is, consequently, probably independent of the background pressure (a conclusion which agrees with ion beam collimation results given by Dalglish and Kelly (1976)).

CHAPTER 5

AN EXPERIMENTAL STUDY OF SPACE CHARGE EFFECTS IN THE 45° PPEA

5.1 Introduction

The influence of space charge effects on the performance of ion energy analyzers has been considered in some detail for several types of electrostatic analyzers (Mason 1964, Fleischmann et al. 1965, Francois and Barat 1968, Green 1970, Chowdhury and Miles 1971, Bryce et al. 1973). However (to the author's knowledge) space charge effects in the PPEA have previously not been treated in detail. Moreover, Chowdhury and Miles (1971) in their examination of techniques used for the ion energy analysis of laser-produced plasmas found that some of the ion energy spectra observed could be explained, at least in part, as being due to space charge effects. Accordingly, we have set out in this chapter, both to illustrate the importance of space charge effects when dealing with laser-produced plasmas, and to provide specific information on the action of space charge effects in the 45° PPEA.

5.2 The Experiment

We have minimized the effects of space charge expansion in the plane parallel to the slits (that is normal to the page in Figure 4.4) by employing an exit slit whose

length (15.0 mm) is an order of magnitude greater than the length of the entrance slit (1.0 mm). To investigate the effects of space charge expansion in the plane normal to the slits (that is, parallel to the page in Figure 4.4) we have incorporated adjustable entrance and exit slit widths in the analyzer (see Appendix B for a description of the slit mechanism). For the results of this chapter, the exit slit width was set at W_{exit} = 0.66 mm, and we have varied the entrance slit width W_{ent}.

For this chapter we have operated so that the laser intensity on target I, is $I = 10^{16}$ Wm^{-2}. Keeping I constant, we found the peaks of the output current pulses first increase linearly with increasing entrance slit width, but then saturate at slit widths wider than some value W_{ent}^{max} (Figure 5.1). From a family of curves similar to Figure 5.1, we deduce Figure 5.2. Inspection of this figure shows that W_{ent}^{max} is approximately independent of E/Z for $E/Z \lesssim 1.0$ keV, but proportional to $(E/Z)^2$ for $E/Z \gtrsim 1.0$ keV.

To illustrate the influence of space charge effects on measured energy spectra, two ion energy spectra are shown in Figure 5.3. Figure 5.3(a) was obtained using a narrow entrance slit width W_{ent} = 0.1 mm, which is smaller than W_{ent}^{max} for all E of interest, while Figure 5.3(b) was obtained using a wide entrance slit width W_{ent} = 2.5 mm, which is larger than W_{ent}^{max} for all E of interest. Figure 5.3(b) is distorted, and clearly for proper operation it

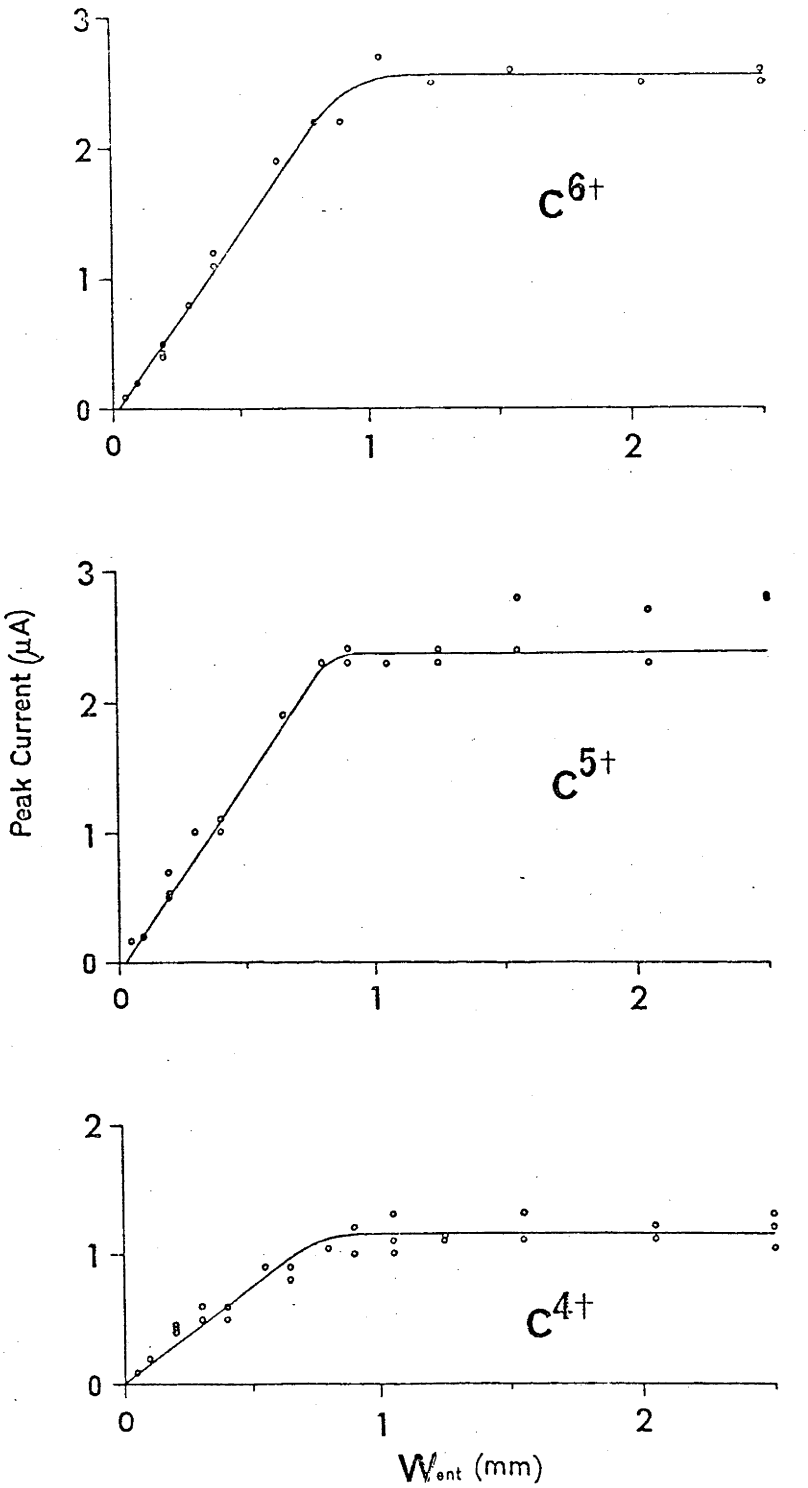

Figure 5.1: Peak ion currents of C^{6+}, C^{5+} and C^{4+} reaching the channel 1 detector as a function of entrance slit width (W_{ent}). The deflecting plate voltage is such that the sampled E/Z ratio is 2.5 keV.

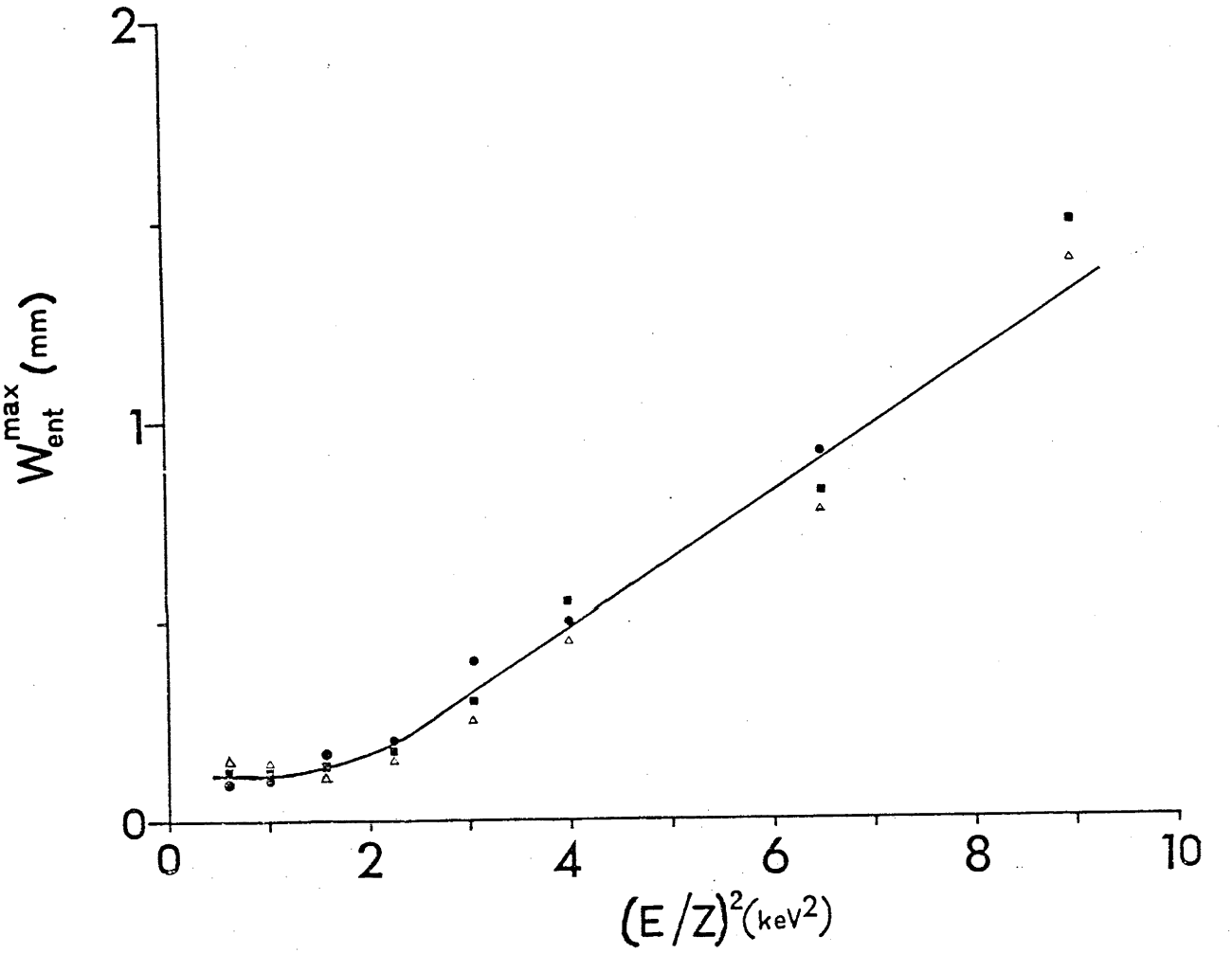

Figure 5.2: The threshold entrance slit width W_{ent}^{max} for onset of output signal saturation plotted as a function of $(E/Z)^2$ for C^{6+} (●), C^{5+} (■), and C^{4+} (▲) ions. A visual curve of best fit is drawn through the points.

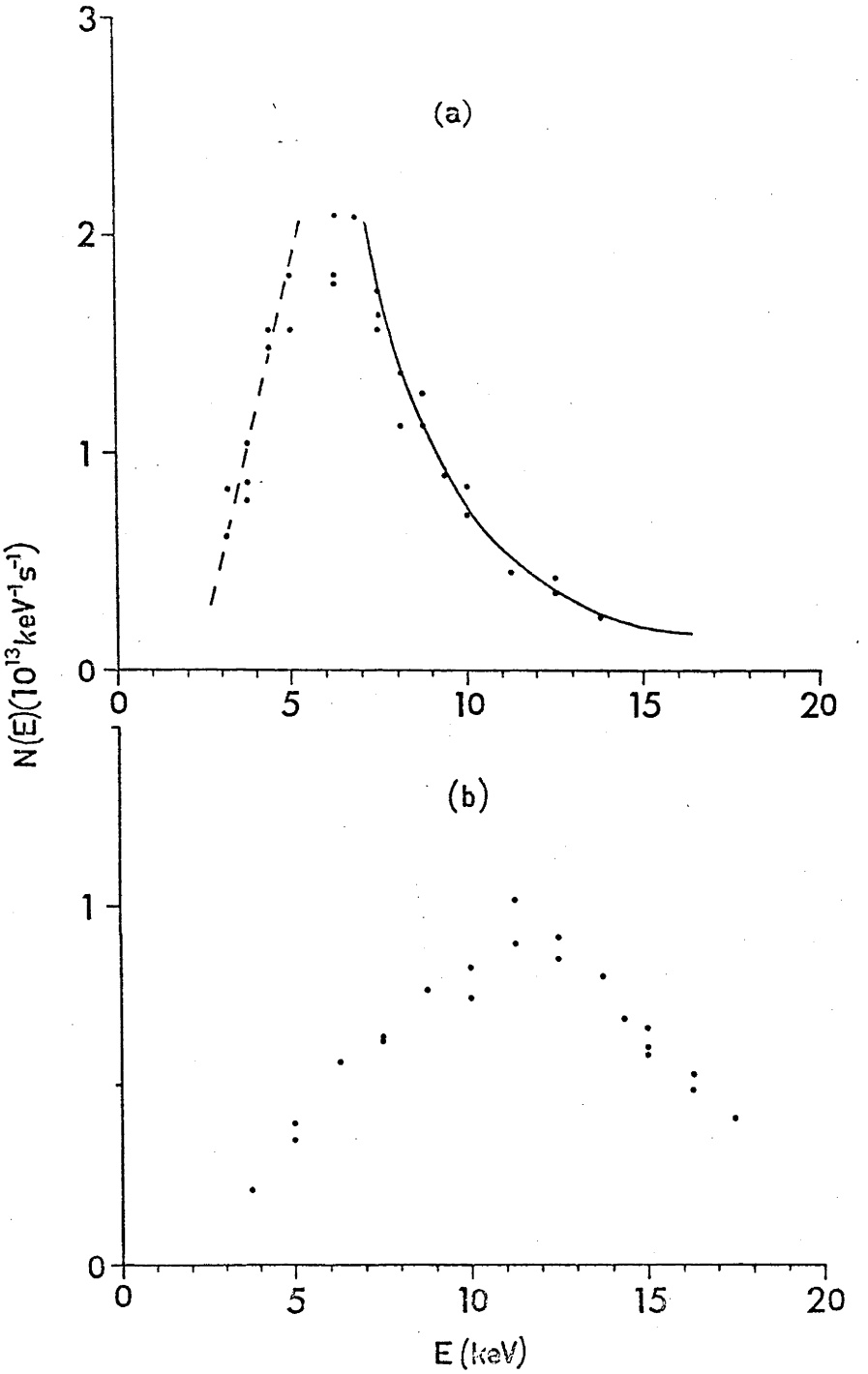

Figure 5.3: Ion energy spectra for C^{5+} ($Z = 5$) obtained using channel 1 with (a) a narrow entrance slit width $W_{ent} = 0.1$ mm $< W_{exit}^{max}$ for all E of interest, and (b) a wide entrance slit width $W_{ent} = 2.5$ mm $> W_{exit}^{max}$ for all E of interest. In (a) the broken curve is a best fit of $N(E) \propto E$ for $E/Z \lesssim 1.0$ keV, while the solid curve is a best fit of $N(E) \propto E^{-3}$ for $E/Z \gtrsim 1.0$ keV (see the discussion in Section 5.3).

is necessary to use the analyzer in the linear region, ie where $W_{ent} < W_{ent}^{max}$.

5.3 Discussion

A theoretical treatment of space charge effects in the 127° deflection analyzer by Fleischmann et al. (1965) assumes the effects are the result of ion beam expansion which can be analytically approximated by the expansion in zero external electric field of a cylindrical mono-energetic ion beam with no initial divergence. Adapting equation (3) of Fleischmann et al. for the 45° PPEA, we have the criterion for proper operation that the entrance slit width W_{ent} is less than W_{ent}^{max}, where

$$W_{ent}^{max} = [\varepsilon_0 E/(n_Z(E)\ e\ Z^2)]^{\frac{1}{2}}\ W_{exit}/x \qquad (5.1)$$

Here $n_Z(E)$ (m^{-3}) is the density of ions of charge Z and energy $E(eV)$ at the entrance slit.

When $E/Z \gtrsim 1.0$ keV, Figure 5.2 shows $W_{ent}^{max} \propto (E/Z)^2$. To derive this variation from equation (5.1) it is necessary to assume $n_Z(E) \propto Z^2/E^3$. For the purpose of illustration Figure 5.3(a) shows for C^{5+} that a curve of the form $N(E) \propto E^{-3}$ gives a fair description of the experimental points for $E/Z \gtrsim 1.0$ keV.

When $E/Z \lesssim 1.0$ keV, Figure 5.2 shows W_{ent}^{max} to be independent of E/Z. To derive this independence from

equation (5.1), it is necessary to assume $n_Z(E) \propto E/Z^2$. As shown again in Figure 5.3(a) a curve of the form $N(E) \propto E$ gives a fair description of the experimental points for $E/Z \lesssim 1.0$ keV.

If for $E/Z \gtrsim 1.0$ keV we write $n_Z(E) = k_1 Z^2/E^3$, and for $E/Z \lesssim 1.0$ keV we write $n_Z(E) = k_2 E/Z^2$, the energy (E_p) where the peak $n_Z(E)$ value occurs is given by $k_1 Z^2/E^3 \simeq k_2 (E_p)/Z^2$, which simplifies to $E_p \simeq (k_1/k_2)^{\frac{1}{4}} Z$. The relation $E_p \propto Z$ is a well-known experimental result for laser-produced plasmas (eg Boland et al. 1968, Paton and Isenor 1968, Demtröder and Jantz 1970).

5.4 Conclusion

Space charge effects within the 45° PPEA cause saturation of the output signal for entrance slit widths wider than some value W_{ent}^{max}. The variation of W_{ent}^{max} with ion energy and charge has been measured and compared with theory. To illustrate the importance of space charge effects on ion energy spectra, a spectrum distorted by space charge effects has been contrasted with the same spectrum free of such effects.

CHAPTER 6

THE ENERGY SPECTRA OF IONS STREAMING FROM A LASER-PRODUCED PLASMA

6.1 Introduction

The energies of ions streaming from laser-produced plasmas have been studied using mainly time-of-flight techniques (eg Linlor 1963, Gregg and Thomas 1966, Opower and Burlefinger 1965, Opower and Press 1966, Boland et al. 1968, Puell et al. 1970, Kang et al. 1972, Dick et al. 1973, Irons et al. 1972, Rumsby and Paul 1974, Ehler 1975, Luther-Davies 1977), and electrostatic and/or magnetic analyzers (eg Langer et al. 1966, Paton and Isenor 1968, Bykovskii et al. 1970, 1971a, b, Olsen et al. 1973, Oron and Paiss 1973, Goforth 1975, Decoste and Ripin 1977). From the results of such papers, it is now well-established that:

(i) the ions acquire a kinetic energy much greater than their initial thermal energy, and

(ii) the average ion kinetic energy is approximately proportional to the ion charge.

Several theoretical treatments have been advanced to explain these and other features of laser-produced plasma ion energy spectra (eg Dawson 1964, Haught and Polk 1966, Hora 1969, Puell 1970, Mattioli 1971, Mulser 1971, Afanas'ev and Rozanov 1972, Allen 1972, Goforth and Hammerling 1976).

In this chapter ion energy and velocity spectra are presented and discussed.

6.2 Data

6.2.1 PPEA

For the results of this chapter we use channel 1 of the PPEA with an exit slit width W_{exit} = 2.5 mm, and an entrance slit width W_{ent} = 0.1 mm. With these slit widths space charges do not affect the analyzer response (see Chapter 5).

Ion energy spectra determined for laser intensities in the range 3×10^{15} to 1.3×10^{16} Wm^{-2} are shown in Figures 6.1 to 6.4. In Figure 6.1 the two-to-four data points recorded for each energy exemplify the shot-to-shot variations. Curves of visual best fit are drawn through the data points. In Figures 6.2 to 6.4 we only show the best fit curves. The insets in Figures 6.1 to 6.4 show the variations with charge of the energies E_p corresponding to the peaks of the energy spectra N(E).

The energy bandwidth (ΔE) sampled by the analyzer decreases with E (see equation 4.2), and for constant N(E) the detector signal to noise ratio correspondingly decreases with E. We did not detect C^{1+} and C^{2+} ions, presumably because C^{1+} and C^{2+} ions have only low energy, and their signal is below the noise level. Given the instrumental

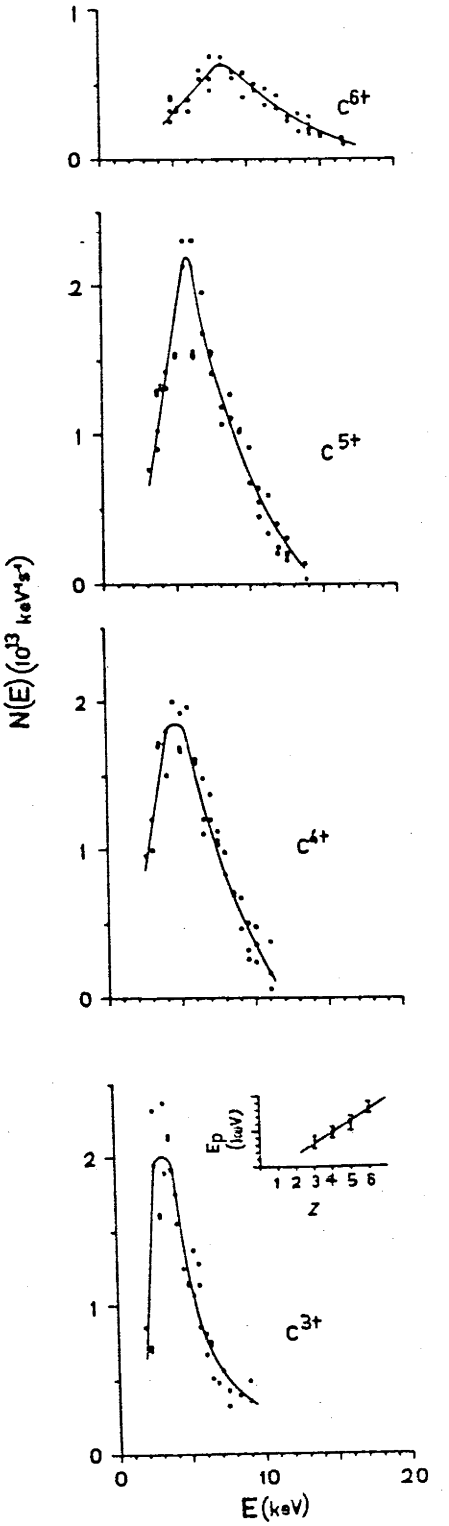

Figure 6.1: Ion energy spectra for different ions (as indicated) as measured with the PPEA for laser intensity on target of 1.3 x 10^{16} W/m^2. Curves of visual best fit are drawn through the experimental points. The inset shows the variation with charge (Z) of the energies E_p where the energy spectra N(E) peak.

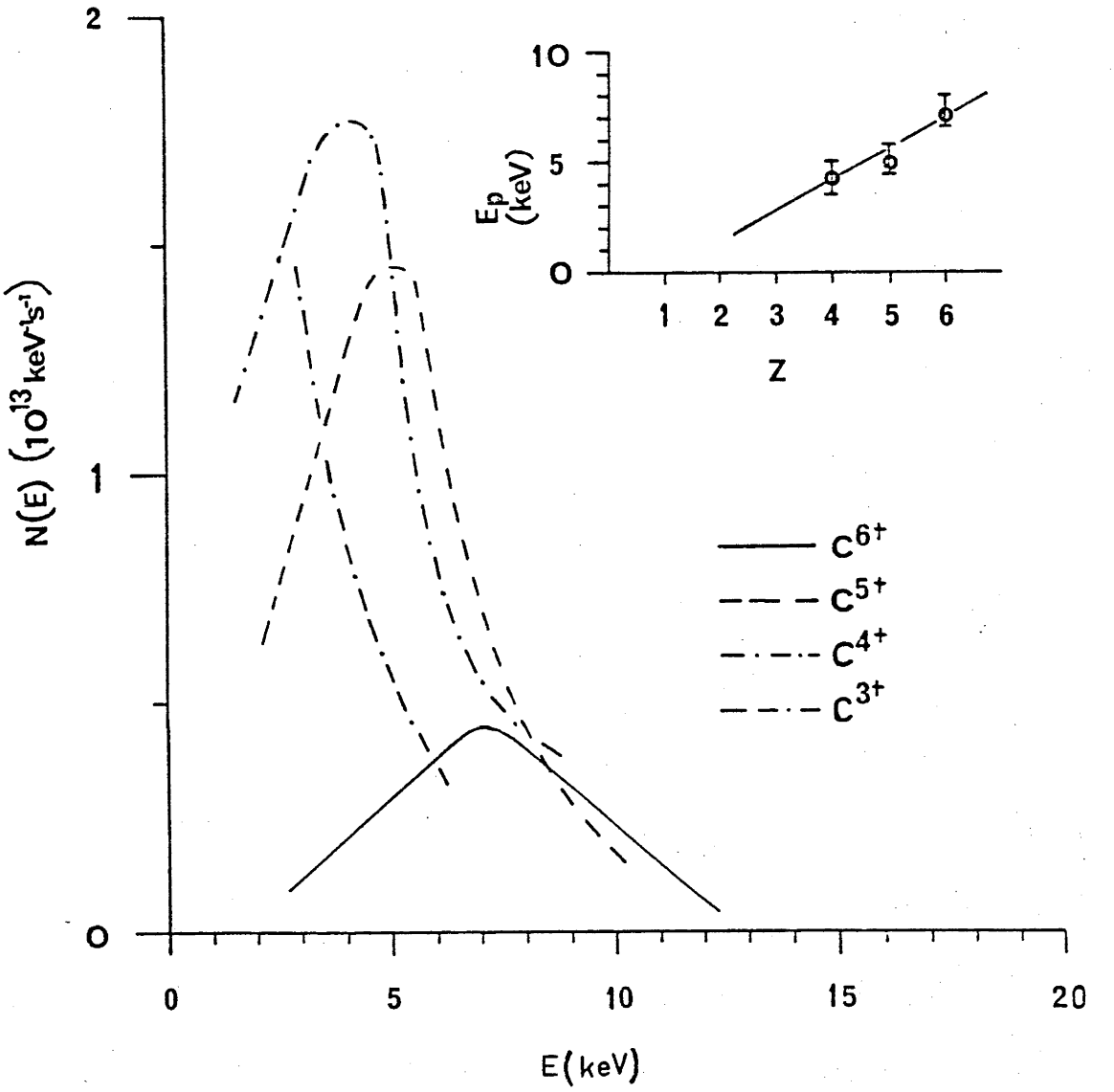

Figure 6.2: Ion energy spectra for different ions (as indicated) as measured with the PPEA for laser intensity on target of 8.4×10^{15} Wm^{-2}. Only the curves of visual best fit are shown. The inset shows the variation with charge (Z) of the energies E_p where the energy spectra N(E) peak.

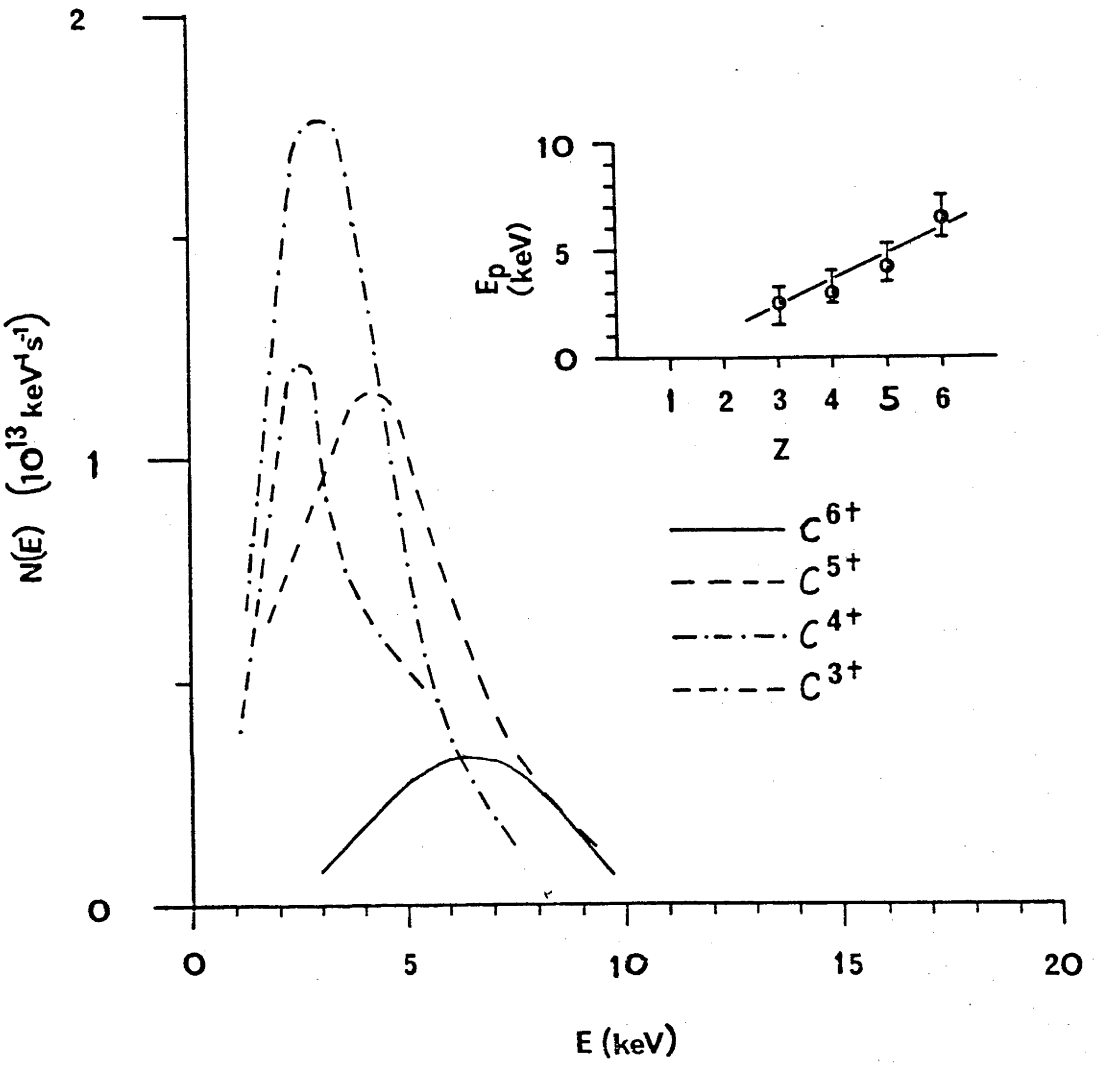

Figure 6.3: As for Figure 6.2, except the laser intensity is 5.5×10^{15} Wm^{-2}.

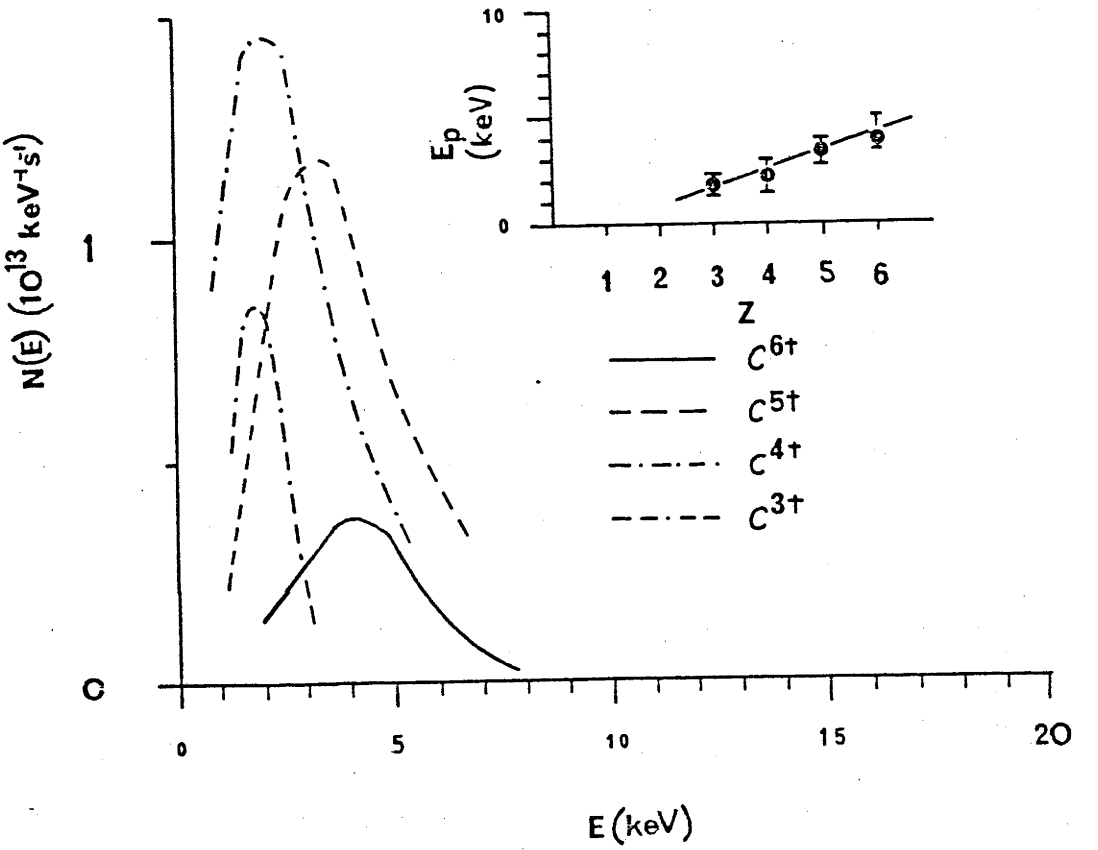

Figure 6.4: As for Figure 6.2, except the laser intensity is 3.2×10^{15} Wm^{-2}.

(Faraday cup, pre-amplifier and oscilloscope) noise level of ≃0.04 μA, we can set an upper limit to N(E = 2 keV) of 1.6 and 0.8 x 10^{13} keV^{-1} s^{-1} for Z = 1 and 2 respectively.

To convert energy spectra N(E) (keV^{-1} s^{-1}) to velocity spectra N(v) ((ms^{-1})$^{-1}$ s^{-1}), we use the relationship N(v) dv = N(E) dE, which gives (with E = ½ $m_i v^2$)

$$N(v) = (2m_i E)^{\frac{1}{2}} N(E) \qquad (6.1)$$

where m_i (kg) is the mass of the ion.

Examples of velocity spectra are presented in Figures 6.5 and 6.6. Data points for C^{6+} at the same velocities are joined by straight lines to indicate the shot-to-shot variation. Figure 6.7 shows the variation with I of the velocities v_p corresponding to the peaks of the velocity spectra N(v). The data points of Figure 6.7 can be fitted with curves $v_p \propto I^{0.2 \pm 0.05}$.

6.2.2 Luminosity times-of-flight

A low dispersion, quartz prism spectrometer (Bellingham and Stanley) with the exit signal monitored by a photomultiplier (EMI 9597 QB) and displayed on an oscilloscope (Tektronix 7844) was used to obtain luminosity times-of-flight close to the target (see Figure 4.3). The plasma axis was imaged onto the spectrometer entrance slit, and the slit masked except for points corresponding to

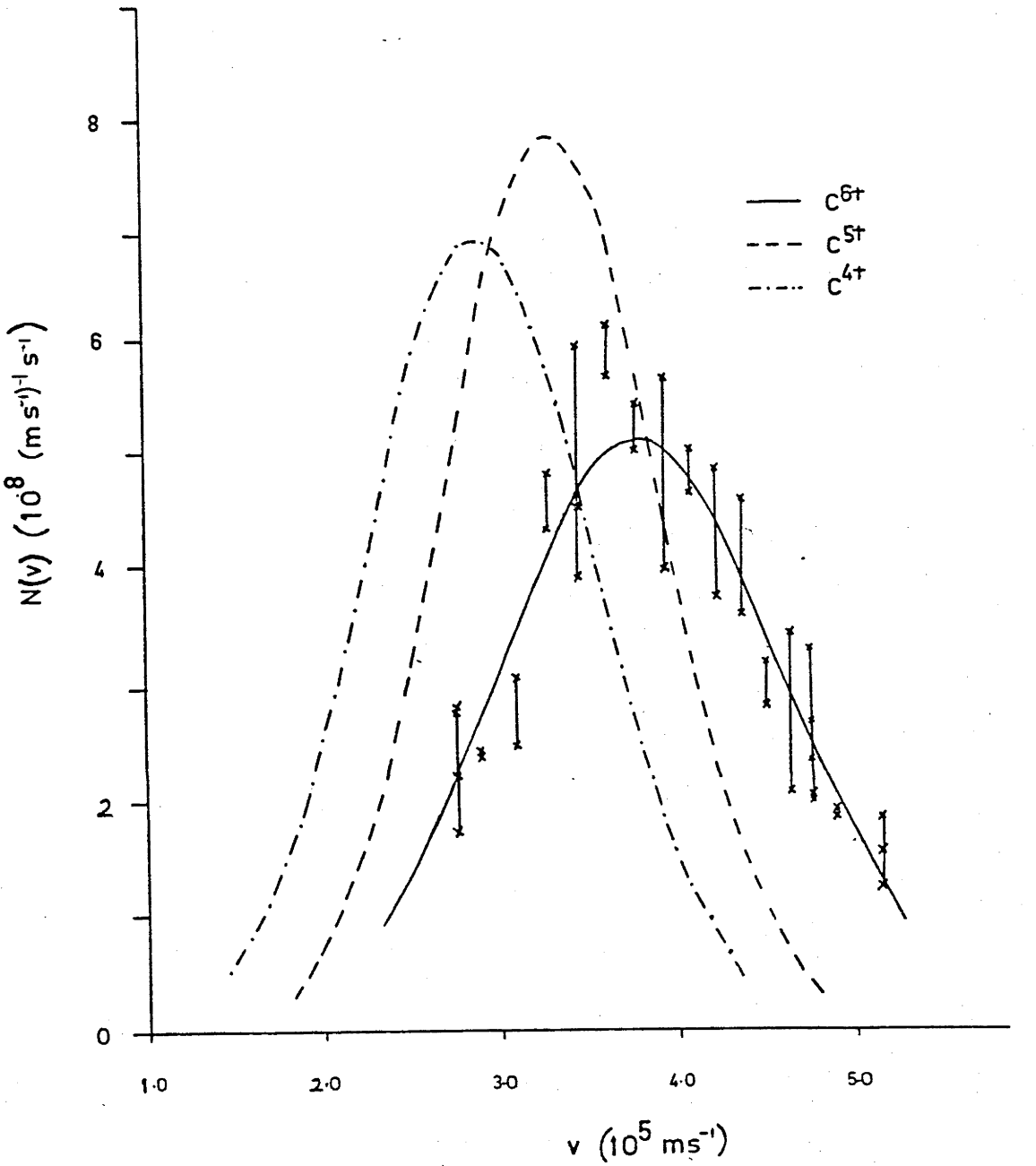

Figure 6.5: Ion velocity spectra for different ions (as indicated), converted from the corresponding energy spectra, for laser intensity on target of 1.3×10^{16} Wm^{-2}. The experimental points for C^{6+} are shown, together with a best fit Maxwellian (superimposed on a drift velocity). For C^{5+} and C^{4+}, only the best fit Maxwellians are shown.

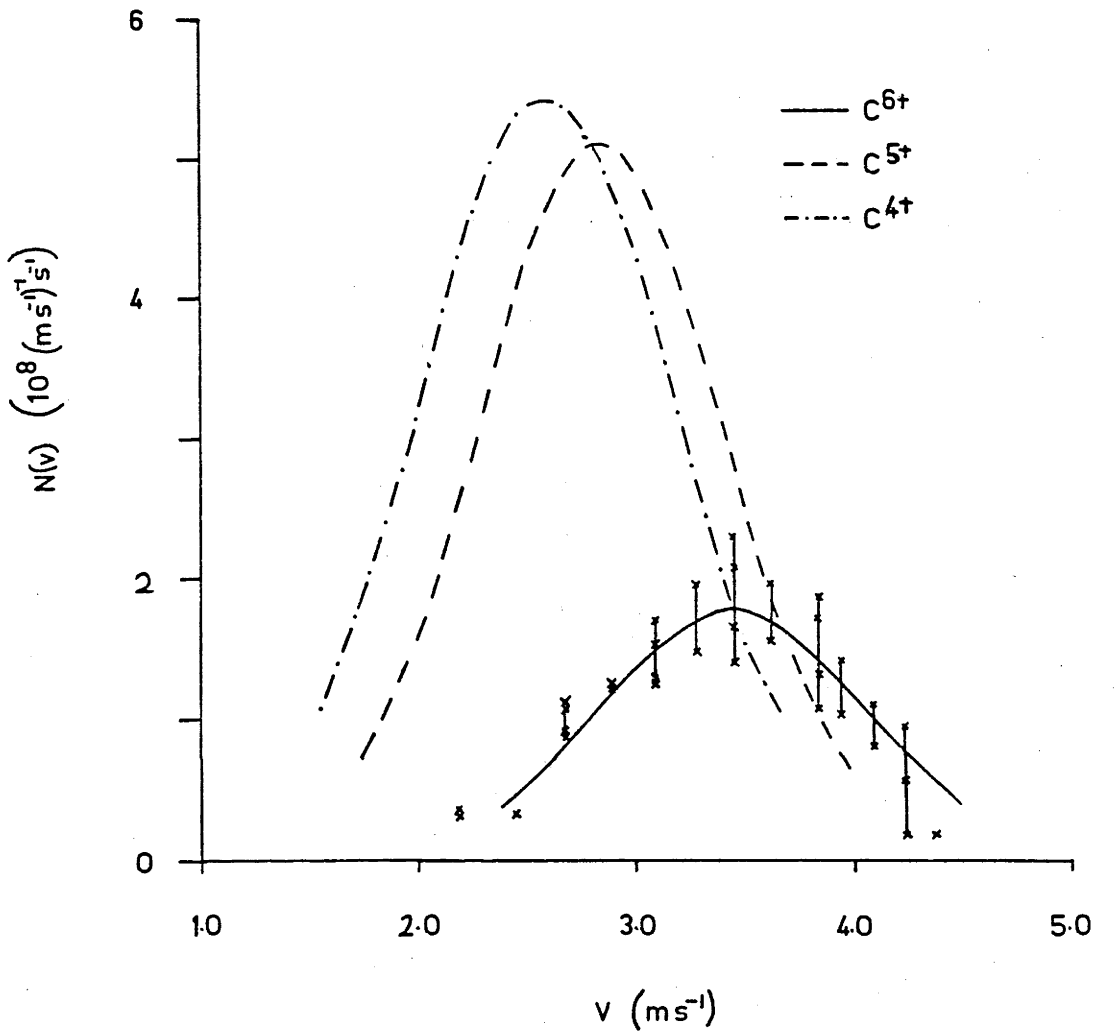

Figure 6.6: As for Figure 6.5, except the laser intensity is 8.4×10^{15} Wm^{-2}.

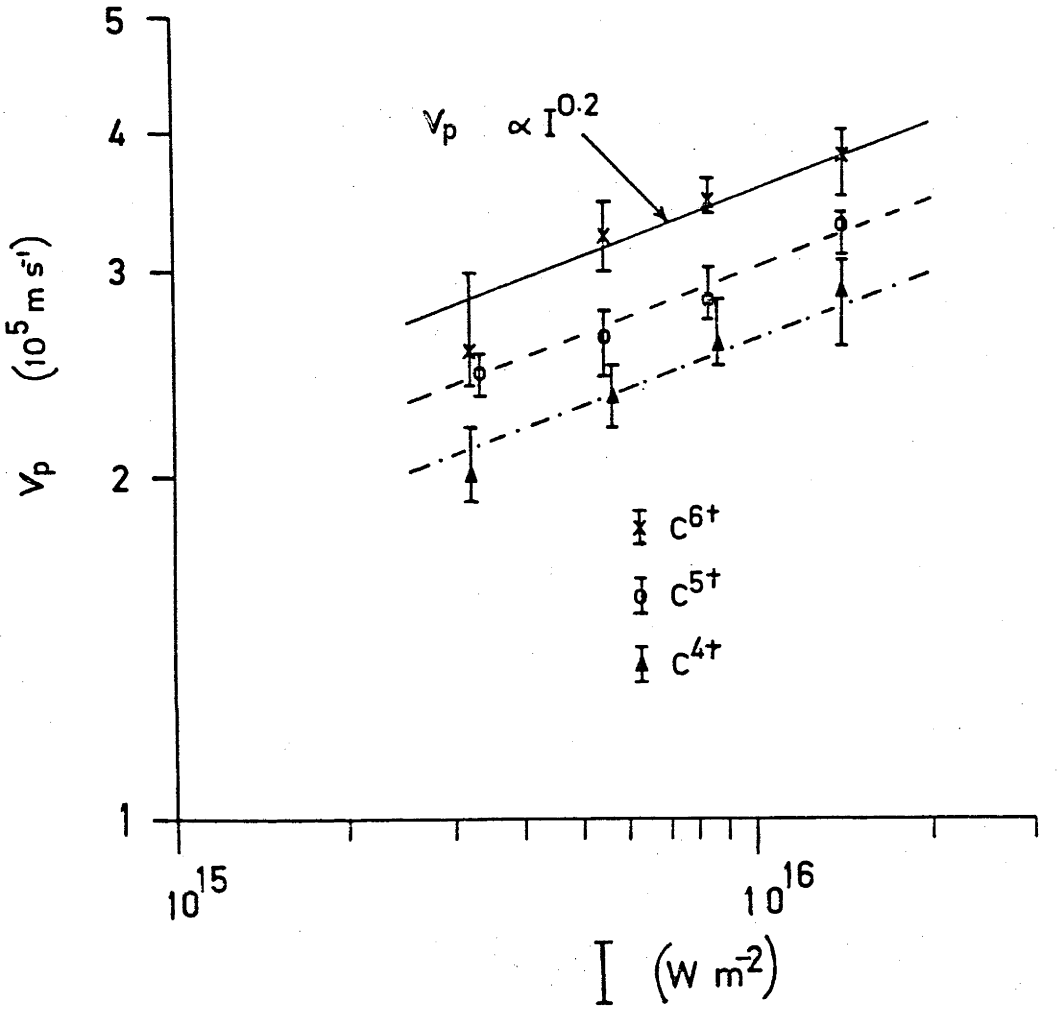

Figure 6.7: Velocities (v_p) where the velocity spectra N(v) peak for C^{6+}, C^{5+} and C^{4+} ions (see eg Figures 6.5 and 6.6), plotted as a function of laser intensity.

TABLE 6.1

Ion velocities determined close to the target (8-16 mm) using luminosity time-of-flight (v_ℓ), and far from the target (800 mm) using the PPEA (v_p) for $I = 1.3 \times 10^{16}$ Wm^{-2}.

Ion Species	v_ℓ (10^5 ms^{-1})	v_p (10^5 ms^{-1})
C^{6+}	$2.9(^{+0.2}_{-0.4})$	$3.8(^{+0.2}_{-0.3})$
C^{5+}	$2.5(^{+0.2}_{-0.4})$	$3.3(^{+0.1}_{-0.3})$

distances 8 mm and 16 mm from the target. By setting the spectrometer to detect the appropriate wavelength, times-of-flight for an 8 mm path length were obtained for CVI ($7 \rightarrow 6$, 3434 Å) and CV ($6 \rightarrow 5$, 2982 Å). Examples of velocities v_ℓ deduced from the times-of-flight are shown for $I = 1.3 \times 10^{16}$ Wm^{-2} in Table 6.1. The velocity v_ℓ was found to vary with I as $v_\ell \propto I^{0.24 \pm 0.04}$ (F E Irons private communications).

6.3 Analysis and Discussion

Several mechanisms have been proposed for the transfer of laser energy to ion kinetic energy in laser-produced plasmas. For example, Hora (1969) has shown that ponderomotive ion acceleration due to gradients in laser intensity can occur. Mulser (1971) assumed an electrostatic field generated by electrons escaping from the plasma accelerated ions to high energy. Allen (1972) has suggested the transfer of excitation energy to kinetic energy by charge exchange and other reactions. A comparative analysis of such mechanisms, however, is beyond the bounds of this thesis, and for the rest of this chapter we mainly confine our attention to the processes occuring after the laser pulse is over. Recombination is discussed in Section 6.3.1. The form of the measured ion velocity distribution is discussed in Section 6.3.2.

6.3.1 Recombination

Recombination takes place with a time constant of

$$t_r = \frac{1}{\alpha N_e} \tag{6.2}$$

where α is the recombination rate coefficient. A comparison of rate coefficients indicates that 3-body recombination dominates 2-body recombination in the expansion plume of a laser-produced plasma (eg Rumsby and Paul 1974). For 3-body recombination we have (Gurevich and Pitaevskii 1964)

$$\alpha \simeq 10^{-38} Z^3 N_e T_e^{-9/2} \ln \sqrt{Z^2 + 1} \tag{6.3}$$

for an ion of initial charge Z, with N_e in m^{-3} and T_e in eV. Upon substituting equation (6.3) into (6.2) we obtain a result which we may write

$$t_r \simeq 10^{38} \frac{N_e \left(T_e N_e^{-2/3}\right)^{9/2}}{Z^3 \ln \sqrt{Z^2 + 1}} \tag{6.4}$$

For an adiabatic expansion, assuming the electrons in a laser-produced plasma behave as an ideal gas, we have, in a volume element, $T_e N_e^{-2/3}$ = constant, and hence from equation (6.4), $t_r \propto N_e$. Setting T_e = 38 eV, $N_e = 4 \times 10^{24}$ m^{-3} (values determined by Irons and Peacock (1974) at 1.0 mm from the target), we have $T_e N_e^{-2/3} = 1.5 \times 10^{-15}$ eV m^2, and hence for C^{6+}

$$t_r \simeq 3 \times 10^{-32} N_e \qquad (6.5)$$

that is, the value of t_r varies from 10^{-7} s at 1.0 mm from the target ($N_e = 4 \times 10^{24}$ m^{-3}), to $\sim 10^{-16}$ s at 800 mm from the target (where $N_e \sim 10^{16}$ m^{-3}). These recombination times are sufficiently short, compared with the expansion time, that we would not expect to observe C^{6+} at 800 mm from the target.

The observation of highly ionized species at large distances from the target can be attributed to the fact that during recombination a certain fraction of the ionization energy is fed to the free electrons. This sustains the electron temperature at a value greater than that in an adiabatic expansion and is responsible for a reduced rate of recombination and thence for a "freezing" of the ion distribution (see Kuznetsov and Raizer 1965, Mattioli 1971, Sklizkov 1971, Goforth and Hammerling 1976).

The quantitative calculations of Goforth and Hammerling, for a plasma model in which the degree of ionization is assumed to be initially spatially uniform, give a valuable physical insight into the effect of recombination (even though the assumption of uniform ionization may not be valid in practice). Additional assumptions of the model are that, initially, the plasma is isothermal with the density decreasing with distance from the target and the streaming velocity increasing with distance from the target.

It emerges from the calculations, that the regions of plasma of initially lower density require less time for the degree of ionization to be frozen. Since the initially lower density regions are the regions of higher velocity, so higher degrees of ionization measured far from the target are associated with higher velocities. This is in agreement with results reported for this thesis (see Figures 6.1 to 6.4), and with other experimental results (eg Boland et al. 1968, Paton and Isenor 1968, Demtröder and Jantz 1970). However, the experimental results may be at least partly due to the fact that, initially, the outermost regions of the plasma which experience the full laser intensity are likely to be the most highly ionized anyway (eg Mulser 1971, Irons et al. 1972).

If, within the one ionization species, the slower ions experience more recombination (Goforth and Hammerling), so the peak in the velocity spectrum of (in this case) C^{6+} may be expected to occur at progressively higher velocities with increasing distance from the target. In this regard note that the (luminosity time-of-flight) velocities observed in the region 8-16 mm from the target amount to only three-quarters of the velocities v_p measured at 800 mm from the target (see Table 6.1).

6.3.2 Ion velocity spectra

A displaced Maxwellian curve of the form

$$N(v) \propto \exp\{-[\frac{m_i (v - v_p)^2}{2kT_t}]\} \qquad (6.6)$$

has been fitted to the various velocity spectra (see eg Figures 6.5 and 6.6). Each spectrum is thus characterised by a "drift velocity" v_p and a "translational temperature" T_t. Plotting T_t as a function of I (Figure 6.8), we find that for C^{6+}, $T_t \propto I$, but that for C^{5+} and C^{4+}, T_t is independent of I. Also shown in Figure 6.8 for the purpose of comparison, are values of electron temperature at the target surface (which we will denote by T_e^{ts}). The T_e^{ts} shown are deduced from the CVI Lyman free-bound continuum by Galanti and Peacock (1975) under experimental conditions (1.06 μm laser radiation focussed onto a polyethylene target) comparable with those used here.

6.3.2.1 T_t-

Several authors have fitted displaced Maxwellian curves of the form in equation (6.6) to ion velocity spectra, and have obtained values of T_t. Allen (1970) used the results of Langer et al. (1966), which were obtained using a Neodymium laser for $I \sim 10^{15}$ Wm^{-2} with an electrostatic analyzer sampling ions streaming at 45° to the target normal. Kang et al. (1972, 1973) (Neodymium laser, $I \sim 10^{16}$ Wm^{-2}) used both a retarding field and an electrostatic analyzer (they did not specify the streaming angle of the ions sampled). Tonon et al. (1971) (Neodymium laser, $I \sim 10^{16}$ Wm^{-2}), and

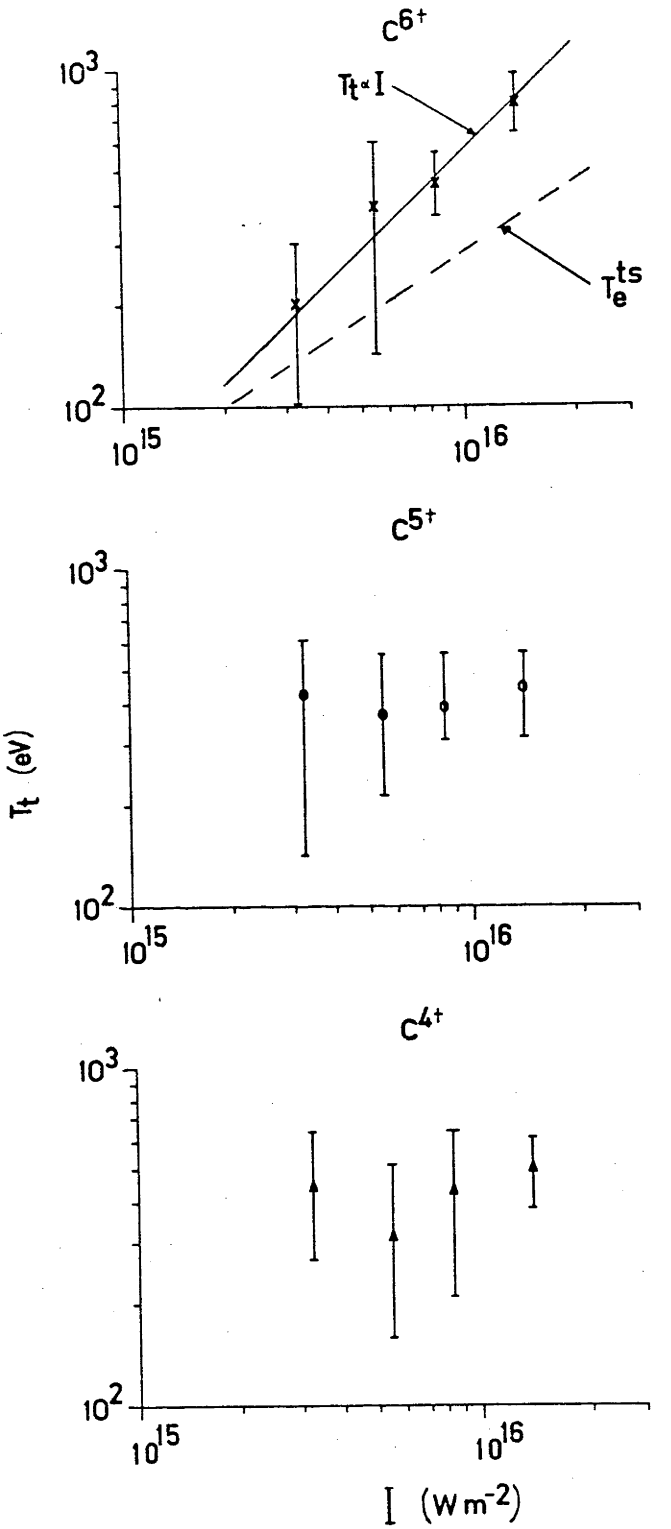

Figure 6.8: Ion translational temperatures (T_t) deduced by fitting Maxwellians superimposed on drift velocities to ion velocity spectra for C^{6+}, C^{5+} and C^{4+} ions, plotted as a function of laser intensity. The best fit curve to the electron temperature (T_e^{ts}) at the target surface deduced by Galanti and Peacock (1975) is shown with the C^{6+} results as a broken line.

Tonon and Rabeau (1973) (CO_2 laser, $I \sim 4\text{-}9 \times 10^{13}$ Wm^{-2}) used the analyzer of Langer et al. (sampling ions streaming at 45° to the target normal). In each of the above cases, the values obtained for T_t were comparable to electron temperatures T_e^{ts} at the target surface.

The inference made in the above papers is that the electron and ion temperatures have equalised at the target surface, and that the ion distribution is frozen into the expanding plasma almost at the very onset of expansion. Tonon and Rabeau (1973) refer to freezing of the degree of ionization, yet, what is inferred in equating T_t to T_e^{ts} (and not discussed in the above paper) is freezing of the ion velocity distribution. Zel'dovich and Raizer (1966) have shown that this is unlikely to occur in any expanding plasma, and indeed from the analysis of Rumsby and Paul (1974) it seems improbable that freezing of the ion velocity distribution occurs in laser-produced plasmas.* As commented by Allen (1970), "one might wonder why the distribution of velocities is more accurately represented

---

* Rumsby and Paul (1974) show that the times which characterise the establishment of an electron temperature T_e, an ion temperature T_i, and the equilibration $T_i = T_e$, all remain constant in an adiabatic expansion with $\gamma = 5/3$. If initially $T_i = T_e$, then in an adiabatic expansion, T_i remains equal to T_e throughout. Ionization energy fed to the electrons by 3-body recombination will cause a departure from adiabatic expansion, with an elevated electron temperature, and a possible decoupling of the electrons from the ions. The electrons decouple from the ions before the ions decouple from one another, and there is then no heat source for the ions, which must expand adiabatically and consequently remain coupled together in a thermal distribution.

by a Maxwellian distribution superposed on a drift speed rather than by a Maxwellian distribution of speeds". The theory of Goforth and Hammerling (1976), which explains some features of the ion velocity spectrum in terms of recombination (see Section 6.3.1), makes no predictions of any relationship between T_t and T_e^{ts}. To summarise, a theoretical case has not been made that T_t should equal T_e^{ts}.

The results in Figure 6.8 show that T_t for C^{6+} departs further from T_e^{ts} with increasing T_e^{ts} (ie with increasing laser power), and that if extrapolated to lower laser powers T_t would equal T_e^{ts} when $T_e^{ts} \approx 80$ eV. We note that the time for equilibration of electron and ion temperatures (Spitzer 1956) at the target surface ($N_e \approx 10^{27}$ m^{-3}) is sufficiently short ($\sim 10^{-10}$ s for C^{6+} ions) for plasmas with the highest temperatures of interest here ($T_e \approx 300$ eV) to achieve equality of electron and ion temperatures. The fact that the relative magnitude of T_t (for C^{6+}) and T_e^{ts} vary with T_e^{ts} can be explained qualitatively as follows. When T_e^{ts} is only marginally above the value required to produce C^{6+}, the drop in T_e at the onset of expansion is accompanied by an initially rapid rate of recombination, by a rapid transfer of ionization energy to the free electrons, and by a rapid freezing of the degree of ionization. At higher initial values of T_e^{ts}, the above processes occur less rapidly at first, allowing more time for net recombination, with a consequently greater effect on the C^{6+} ion velocity distribution

Regarding T_t for C^{5+} and C^{4+}, the fact that T_t is largely independent of I

(see Figure 6.8) can be explained by noting that the ion velocity spectra for C^{5+} and C^{4+} are complicated by recombination to these species, as well as from these species, and with changing T_e^{ts} each process compensates the other to result in T_t (for C^{5+} and C^{4+}) being constant with T_e^{ts}, and consequently with I.

6.3.2.2 V_p

Most models of laser-plasma interaction which assume the laser light is absorbed in the plasma corona predict "drift velocities" $\alpha\ I^{0.22}$ (eg Caruso and Gratton 1968, Puell 1970). Models assuming absorption only at the critical density predict velocities varying around $I^{0.33}$ (eg Fauquignon and Floux 1970). Identifying our v_p ($\alpha\ I^{0.2 \pm 0.05}$) and v_ℓ ($\alpha\ I^{0.24 \pm 0.04}$) with the velocities of these calculations, we see that our results agree with models which assume the laser light is absorbed in the plasma corona, but are not in agreement with models assuming only absorption at the critical density.

CHAPTER 7

CONCLUSION

In Part I we have discussed mechanisms for achieving population inversion amongst the quantum states of hydrogen-like ions in a rapidly cooling plasma such as a laser-produced plasma. Population densities of excited and ground states of hydrogen-like ions have been computed on a time-dependent basis for an initially steady-state plasma in which the electron temperature subsequently decays exponentially with a half-life sufficiently short ($\sim 10^{-13}$ s) to produce population inversions with respect to the ground state. The principal results are for $Z = 6$ (C^{5+}), initial electron temperature 200 eV and electron density 10^{21} cm^{-3}, though variations in these parameters are considered. We have shown that the necessary cooling rates for inversion with respect to the ground state may be achieved in very small plasmas, but are unlikely to be achieved in laser-produced plasmas in the absence of compression or self-focusing.

We have investigated the effect in laser-produced plasmas of Lyman α self-absorption on quasi-steady state population inversions between quantum states $n = 2$ and 3 of hydrogen-like ions, again with particular reference to $Z = 6$ (C^{5+}). Using the computer code COLLRAD (described in Appendix A), we showed how the electron density range

over which 3 → 2 population inversions are possible reduces as Lyman α self-absorption increases.

In Part II we have discussed the operation and results from a 45° parallel plate electrostatic analyzer built to measure the energies of ions streaming from a laser-produced plasma. Space charge effects in the analyzer were found to cause saturation of the output signal for entrance slit widths wider than values W_{ent}^{max}, and the variation of W_{ent}^{max} with ion energy and charge was measured and compared with theory. Energy spectra of ions (C^{3+}, C^{4+}, C^{5+} and C^{6+}) streaming along the normal to the target surface have been presented for laser intensities in the range 3×10^{15} to 1.3×10^{16} Wm^{-2}. The role of recombination in forming these spectra has been discussed.

The work described in Parts I and II is interrelated as outlined in Chapter 1, and represents part of an ongoing program of work in this laboratory. The next step is to repeat the ion velocity measurements at a number of angles to the target normal, thereby obtaining information on the differential in the component of ion streaming velocity transverse to the target normal. This information is needed for the interpretation of optically thick line intensities, as mentioned in Chapter 1. The body of data obtained could also provide a starting point for a theoretical evaluation of the angular distribution of the different ionization species.

APPENDICES

APPENDIX A

COLLRAD: a code for calculating the quasi-steady state population densities of excited states of hydrogen-like ions

Computer Physics Communications 12 (1976) 205–212
© North-Holland Publishing Company

COLLRAD: A CODE FOR CALCULATING THE QUASI-STEADY STATE POPULATION DENSITIES OF EXCITED STATES OF HYDROGEN-LIKE IONS

G.J. TALLENTS

Department of Engineering Physics, Research School of Physical Sciences, The Australian National University, Canberra, A.C.T. 2600, Australia

Received 6 October 1976

PROGRAM SUMMARY

Title of program: COLLRAD

Catalogue number: AAID

Program obtainable from: CPC Program Library, Queen's University of Belfast, N. Ireland (see application form in this issue)

Computer: UNIVAC 1108 and 1100/42; *Installation*: Australian National University, Canberra

Operating system: EXEC-8

Programming language used: FORTRAN

High speed store required: 14620 words

No. of bits in a word: 36

Overlay structure: None

No. of magnetic tapes required: None

Other peripherals used: Line printer, card reader

No. of cards in combined program and test deck: 1360

Card punching code: EBCDIC

Keywords: Collisional, radiative, recombination, ionization, hydrogen-like, population density, plasma, spectroscopy, atomic, astrophysics.

Nature of physical problem
The evaluation of the population densities of the lower quantum states of a plasma ion, in general, involves the simultaneous solution of the rate equations (one for each quantum state) containing the rates of the various collisional and radiative processes which populate and de-populate each quantum state. We consider the time independent case where quasi-steady state equilibrium is established.

Method of solution
COLLRAD calculates quantum state densities for hydrogen-like ions using the collisional-radiative model of Bates et al. [1] and McWhirter and Hearn [2]. Coefficients giving the population densities of the excited states, and the rate of change of the ground state density are calculated for input electron density and temperature by solving a set of simultaneous linear equations.

Restrictions on the complexity of the problem
Densities are calculated for excited quantum states in quasi-steady state equilibrium.

Typical running time
For execution 1.7 sec on the ANU UNIVAC 1100/42.

Unusual features of the program
COLLRAD is written in standard FORTRAN, except for the use of the NAMELIST facility.

References
[1] D.R. Bates, A.E. Kingston and R.W.P. McWhirter, Proc. Roy. Soc. A267 (1962) 297.
[2] R.W.P. McWhirter and A.G. Hearn, Proc. Phys. Soc. 82 (1963) 641.

LONG WRITE-UP

1. Introduction

In an optically thin plasma, spectral line intensities are proportional to the population densities of excited quantum states. There have, consequently, been many publications dealing with the evaluation of excited quantum state densities, both for "equilibrium" situations (e.g. the coronal model and the Saha–Boltzmann equation, see refs. [1] and [2]), and "general" situations (e.g. refs. [3]–[14]). The general evaluations, which concern us here, involve the consideration of the rates of all significant collisional and radiative processes populating and de-populating each quantum state, and require a computer.

COLLRAD is a computer code which calculates excited quantum state densities for hydrogen-like ions. The collisional–radiative quasi-steady state model of Bates et al. [3] and McWhirter and Hearn [6] is followed. The code uses the rate coefficients for populating and de-populating processes given or cited in Bates et al. [3], though overriding user-supplied collisional rate coefficients can be input.

2. Theory

2.1. The basic equation

The collisional and radiative processes which are included in the code are the following:

(1) Excitation of a hydrogen-like ion of nuclear charge Z from a quantum state n to a quantum state m by electron impact, and the inverse process of de-excitation

$$H_n^{(z-1)+} + e \rightleftharpoons H_m^{(z-1)+} + e \,.$$

The rate coefficients for the forward and backward process are given the symbols $K(n, m)$ and $K(m, n)$ (units $cm^3\ sec^{-1}$) in this text, and represented by the array elements AKD(N, M) and AKD(M, N) in the code.

(2) Collisional ionization of the ion from a quantum state n and the inverse process of three-body recombination

$$H_n^{(z-1)+} + e \rightleftharpoons H^{z+} + e + e \,.$$

The rate coefficients are given the symbols $K(n, c)$ and $K(c, n)$ (units $cm^3\ sec^{-1}$), respectively, in this text, and represented by the vector elements AKION(N) and AKREC(N) in the code.

(3) Spontaneous radiative decay from a quantum state n to a lower quantum state m

$$H_n^{(z-1)+} \rightarrow H_m^{(z-1)+} + h\nu \,.$$

The transition probability is denoted $A(n, m)$ (sec^{-1}) in this text, and by APROB(N, M) in the code. The inverse process of photo-excitation is considered by using the optical escape factor $\Lambda(n, m)$ [15]: the code multiplies the transition probability A by an escape factor $\Lambda \leqslant 1$, and so reduces the spontaneous radiative decay probability to an effective value $[= \Lambda(n, m)\, A(n, m)]$ which includes the effect of any photo-excitation. The escape factor values are user-specified using a code number (LDEPTH) for the assumed degree of line radiation self-absorption.

(4) Radiative recombination of an electron with a bare (fully stripped) nucleus to form an ion in quantum state n

$$H^{z+} + e \rightarrow H_n^{(z-1)+} + h\nu \,.$$

The rate coefficient is denoted $\beta(n)$ $cm^3\ sec^{-1}$ in this text, and BETA(N) in the code. The inverse of this process, namely photo-ionization, can be neglected.

It is assumed that the discrete quantum states are adequately specified by their principal quantum numbers and that the sub-states are populated according to their statistical weight. Generally, the rate of collision induced transitions between the sub-states is sufficiently large to ensure this.

Given the above-mentioned processes, the population density of quantum state n, namely N_n (cm^{-3}) changes at a rate

$$\frac{dN_n}{dt} = -N_n \left[N_e \left(K(n, c) + \sum_{m \neq n} K(n, m)\right)\right.$$

$$\left. + \sum_{m<n} \Lambda(n, m) A(n, m)\right] + N_e \sum_{m \neq n} N_m K(m, n) \quad (1$$

$$+ \sum_{m>n} N_m \Lambda(m, n) A(m, n) + N_e^2 / X [K(c, n) + \beta(n)]$$

where N_e (cm^{-3}) is the free electron density, and X is the ratio of N_e to the number density of bare nuclei of charge Z.

2.2. The quasi-steady state solution

The variation of the quantum state densities is controlled by a large number of differential equations (1), one for each discrete quantum state. However, when a plasma initially in the steady state ($dN_n/dt = 0$ for all n) is perturbed, dN_n/dt ($n > 1$) returns to zero much more quickly than dN_1/dt [6,15], and to calculate the excited quantum state densities we can set $dN_n/dt = 0$ ($n > 1$) (the $n > 1$ quantum states are then said to be quasi-steady state).

The calculation of the population densities N_n can be reduced further in complexity by noting that high quantum states ($n > n'' = 20$) are populated according to the Saha–Boltzmann equation [3]

$$N_n^E = 4.2 \times 10^{-16} \frac{N_e^2}{X} \frac{n^2}{T_e^{3/2}} \exp\left(\frac{157\,890\, Z^2}{n^2 T_e}\right) \qquad (2)$$

where N_n^E (cm^{-3}) is the Saha–Boltzmann population density for quantum state n, and T_e(K) is the electron temperature.

Expressing eq. (1) ($dN_n/dt = 0, n = 2, 3, 4, \ldots n''$) in matrix form we have

$$\underset{(n''-1)\times(n''-1)}{\mathbf{D}_{(n''-1)}}\mathbf{N}_{(n''-1)} + \mathbf{B}_{(n''-1)} + \mathbf{C}_{(n''-1)}N_1 = \mathbf{0}_{(n''-1)}, \qquad (3)$$

where

$$D(n-1, m-1) = \begin{cases} N_e K(m, n) & (m<n), \\ -N_e\left(K(n, c) + \sum_{l\neq n} K(n, l)\right) & \\ \quad - \sum_{l<n} \Lambda(n, l) A(n, l) & (m=n), \\ N_e K(m, n) + \Lambda(m, n) A(m, n) & (m>n) \end{cases}$$

$$B(n-1) = N_e^2/X\,[K(c, n) + \beta(n)] + \sum_{l>n''} N_l^E\,[N_e K(l, n) + \Lambda(l, n) A(l, n)],$$

$$C(n-1) = N_e K(1, n),$$

and $\mathbf{N}$ is a vector with elements equal to the population densities for quantum states $n = 2, 3, 4, \ldots, n''$. Solving eq. (3) for $\mathbf{N}$ gives the quasi-steady state population densities of the excited quantum states. However, eq. (3) contains the ground quantum state population density, so any deduced N_n values are functions of N_1. Expressing the population densities as functions of the Saha–Boltzmann populations we write

$$N_n/N_n^E = r_0(n) + r_1(n)(N_1/N_1^E), \qquad (4)$$

where $r_0(n)$ and $r_1(n)$ are two coefficients [denoted by R0(N) and R1(N) in the code].

The rate of change with time of the ground quantum state density can also be expressed in terms of two coefficients, the effective three-body recombination coefficient α ($cm^3\ sec^{-1}$), and the effective three-body ionization coefficient S ($cm^3\ sec^{-1}$) (denoted by ALPH and S in the code)

$$dN_1/dt = (N_e^2/X)\alpha - N_e N_1 S \cdot \qquad (5)$$

The quasi-steady state solution of population densities is valid for most plasmas of laboratory or astrophysical interest. Exceptions occur when plasma conditions change very rapidly [16–21], or when at low electron densities there is significant self-absorption of line radiation [4,5,8].

2.3. The rate coefficients

To solve eq. (3) numerically it is necessary to assign values to the rate coefficients K, A and β. In the code the radiative recombination coefficients $\beta(n)$ are calculated using the data of table 1 of Seaton [22] (the data in this table is provided with the code). The Einstein transition probabilities $A(n, m)$ are calculated from absorption oscillator strengths $f(m, n)$, namely

$$A(n, m)_{n>m} = 8.03 \times 10^9\, Z^4 \left[\frac{1}{m^2} - \frac{1}{n^2}\right] \frac{m^2}{n^2} f(m, n) \cdot \qquad (6)$$

The $f(m, n)$ values for $n \leqslant 25, m \leqslant 20$ need to be input to the code (the data from Wiese et al. [23] is provided with COLLRAD). For $n > 25$ the code uses the following asymptotic formula for the oscillator strength [3]:

$$f(m, n)_{n>m} = 1.96\,[n^3 m/(n^2 - m^2)^3] \cdot \qquad (7)$$

The radiative rate coefficients A and β for hydrogen-like ions are known to high precision, but this is not the case with the collisional rate coefficients K. Consequently, COLLRAD allows user-supplied K coefficients to be input. The default values are the following collisional rate coefficients for hydrogen-like ions taken from Bates et al. [3]:

$$K(n, m)_{m>n} = 4.75 \times 10^{-5} \frac{n^2 m^2}{m^2 - n^2} \frac{f(n, m)}{Z^2 T_e^{1/2}} \times \exp\left\{\frac{-157\,890\, Z^2 (m^2 - n^2)}{m^2 n^2 T_e}\right\} \quad (8)$$

$$K(n, c) = \frac{1.4 \times 10^{-5} n^2}{Z^2 T_e^{1/2}} \exp\left\{\frac{-157\,890\, Z^2}{n^2 T_e}\right\} . \quad (9)$$

The default rate coefficients for the reverse transitions $K(m, n)$ $(m > n)$, $K(c, n)$ are calculated using detailed balancing.

2.4. Scaling of results

With the values for K, A and β given in section 2.3, the dependence of eq. (3) on Z and X may be included by substituting the reduced parameters [6]:

electron temperature $\theta = T_e/Z^2$, (10)

electron density $\eta_e = N_e/Z^7$, (11)

population density $\eta_n = N_n X/Z^{11}$. (12)

The effective recombination and ionization coefficients then also scale with Z, and we can introduce reduced values [3]:

effective recombination coefficient

$$\Gamma = \alpha/Z^2 , \quad (13)$$

effective ionization coefficient

$$\sigma = SZ^3 . \quad (14)$$

The coefficients $r_0(n)$, $r_1(n)$ are independent of Z and X for given θ, η_e.

3. Structure of the code and instructions for users

A flow diagram of COLLRAD is shown in fig. 1 and an index of subprograms is given in table 1. In subroutine PLASMP the code inputs (using NAMELIST "INPUT", see table 2) the plasma parameters TEMP (T_eK), EDNSTY (N_e cm^{-3}), X and AZED (Z), plus the integer variables LIM ($= n''$, discussed in section 2.2) and LDEPTH (discussed in section 2.1). LDEPTH is a code number for the assumed degree of line radiation self-absorption (e.g. the default of zero implies all lines are optically thin, see table 2).

In subroutine MODIFY the code can input (using NAMELIST "RCMOD") the collisional rate coefficients AKD (n, m) [$K(n, m)$ cm^3 sec^{-1}], AKION (n) [$K(n, c)$ cm^3 sec^{-1}] and AKREC (n) [$K(c, n)$ cm^3 sec^{-1}]. If no input is made for a particular coefficient the default value is used (see section 2.3). There are, however, two options here for COLLRAD (see fig. 1). With option (1) only $K(n, m)$ $(m > n)$ and $K(n, c)$ coefficients should be input. $K(m, n)$ $(m > n)$ and $K(c, n)$ are calculated using detailed balancing. With option (2) any collisional rate coefficients can be input, and inverse processes (except those set by default) are not necessarily in detailed balance. The code pre-

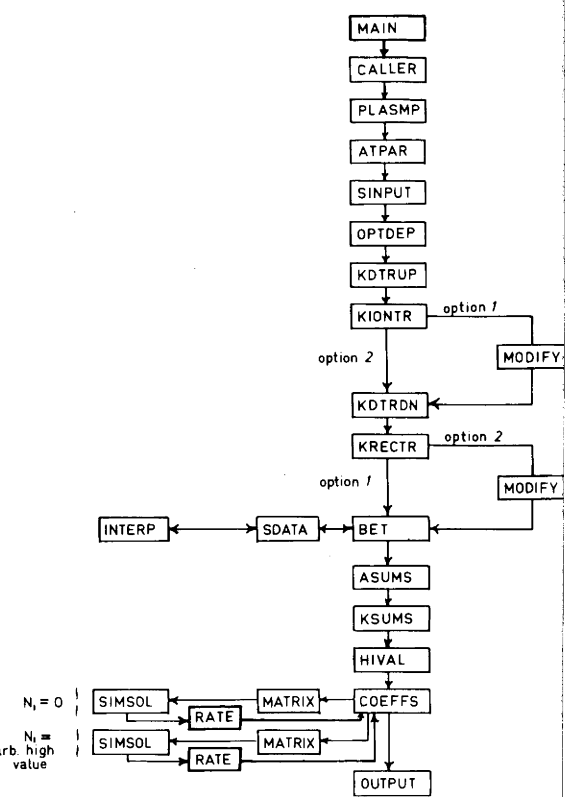

Fig. 1. The COLLRAD flow diagram.

Table 1

ndex of subprograms (taken from the COLLRAD listing)

CALLER	Calling subroutine
PLASMP	Input plasma parameters
ATPAR	Input atomic parameters
SINPUT	Input radiative recombination data
OPTDEP	Allow for self-absorption of line radiation
CDTRUP	Calculate rate coefficients for upward collision induced discrete transitions
CIONTR	Calculate rate coefficients for collision induced ionization
MODIFY	Input any revised collisional rate coefficients over-riding the calculated values
CDTRDN	Use detailed balancing to calculate downward collision induced discrete transition rate coefficients
CRECTR	Use detailed balancing to calculate collision induced (three-body) recombination rate coefficients
BET	Calculate radiative recombination rate coefficients
SDATA	Calculate coefficients for the evaluation of the Kramers-Gaunt factor used to calculate the radiative recombination rate coefficients
INTERP	Interpolate input data for 'SDATA' evaluation
ASUMS	Sum radiative transitions out of each quantum state
KSUMS	Sum collisional transitions out of each quantum state
HIVAL	Sum recombination rates from high (GT. 'LIM') quantum states to lower (LE. 'LIM') states
COEFFS	Evaluate 'R0 'R1', 'ALPH' and 'S' Coefficients
MATRIX	Calculate elements of matrices for the matrix equation whose solution gives the densities of the quantum states
SIMSOL	Solve the matrix equation to give population densities of the quantum states
RATE	Calculate the rate of change with time of the ground state population density
OUTPUT	Output the 'R0', 'R1', 'ALPH' and 'S' coefficients

sented to the CPC library is in the option (1) form, but can be readily changed to option (2) by following instructions given in subroutine CALLER.

Using conventional format statements, input of (i) the absorption oscillator strengths $f(m, n)$ ($n \leqslant 25$, $m \leqslant 20$), and (ii) the data from table 1 of Seaton [22] is required in respective subroutines ATPAR and SINPUT. When using the code it is necessary to always add this data (which is provided with the code when ordered from CPC) to the runstream in the appropriate position. Table 3 shows the order of data read by the code.

Table 2

Contents of NAMELIST 'INPUT' (taken from the COLLRAD listing)

Name	Function (units)	Default value
AZED	Atomic number	1.0
EDNSTY	Electron density (cm^{-3})	1.0×10^{14}
LDEPTH	Code number indicating the line radiation self-absorption in the plasma	0
	0 Plasma optically thin (all $\Lambda = 1$)	
	1 L_α 10% absorbed ($\Lambda(2, 1) = 0.9$)	
	2 L_α 50% absorbed ($\Lambda(2, 1) = 0.5$)	
	3 L_α 90% absorbed ($\Lambda(2, 1) = 0.1$)	
	4 L_α 99% absorbed ($\Lambda(2, 1) = 0.01$)	
	5 L_α 99.9% absorbed ($\Lambda(2, 1) = 0.001$)	
	6 L_α 100% absorbed ($\Lambda(2, 1) = 0.0$)	
	10 Lyman series 10% absorbed ($\Lambda(n, 1) = 0.9$)	
	11 Lyman series 50% absorbed ($\Lambda(n, 1) = 0.5$)	
	12 Lyman series 90% absorbed ($\Lambda(n, 1) = 0.1$)	
	13 Lyman series 99% absorbed ($\Lambda(n, 1) = 0.01$)	
	14 Lyman series 99.9% absorbed ($\Lambda(n, 1) = 0.001$)	
	15 Lyman series 100% absorbed ($\Lambda(n, 1) = 0.0$)	
	20 All lines absorbed (all $\Lambda = 0.0$)	
LIM	Population densities for quantum states above 'LIM' are assumed to be Saha-Boltzmann. 'LIM' must be less than or equal to 20	20
TEMP	Electron temperature (K)	32,000
X	(Electron density)/(Bare nuclei density)	1.0

The code outputs (in subroutine OUTPUT) the coefficients $r_0(n)$, $r_1(n)$ ($n = 2, 3, 4, \ldots, n''$), α, S and the Saha–Boltzmann densities N_n^E ($n = 1, 2, 3, \ldots, n''$).

Table 3
The data input for COLLRAD

(1) $INPUT ... $END	NAMELIST variables in 'INPUT'
(2) 290 lines of absorption oscillator strengths 50 lines of radiative recombination data	This is standard data and should be added to the runstream unchanged.
(3) $RCMOD ... $END	NAMELIST variables in 'RCMOD'

Setting $Z = X = 1$ does not produce results for atomic hydrogen; the COLLRAD results apply to hydrogen-like ions only. Results for atomic hydrogen need to be calculated using a different set of collisional rate coefficients. With $Z = X = 1$ the code operates with reduced parameters and outputs $r_0(n), r_1(n), \Gamma, \sigma$ and η_n^E for input θ, η_e.

4. Testing the code

A user can test COLLRAD by reproducing published results. As an example, we present the code print-out for an optically thin plasma with T_e = 8000 K, $N_e = 10^{14}$ cm^{-3}, $Z = 1$, $X = 1$ (setting $Z = X = 1$ results in reduced values being output by the code, see section 3). For the sample print-out we used the collisional rate coefficients of refs. [3] and [6] which at θ = 8000 K, $\eta_e = 10^{14}$ cm^{-3} are the COLLRAD default values except for the following (taken from table 1 of ref. [6]: the rate coefficients of table 1 ref. [6] were used in ref. [3], although this was not stated in ref. [3]–[24]).

$K(1, 2) = 6.20 \times 10^{-14}$ cm^3 sec^{-1},
$K(2, 1) = 4.16 \times 10^{-8}$ cm^3 sec^{-1},
$K(1, 3) = 8.41 \times 10^{-16}$ cm^3 sec^{-1},
$K(3, 1) = 3.89 \times 10^{-9}$ cm^3 sec^{-1},
$K(1, 4) = 1.37 \times 10^{-16}$ cm^3 sec^{-1},
$K(4, 1) = 9.29 \times 10^{-10}$ cm^3 sec^{-1},
$K(1, c) = 4.90 \times 10^{-17}$ cm^3 sec^{-1},
$K(c, 1) = 1.07 \times 10^{-15}$ cm^3 sec^{-1}.

The COLLRAD deduced coefficients $r_0(n), r_1(n)$, Γ and σ for θ = 8000 K, $\eta_e = 10^{14}$ cm^{-3} given in the sample print-out are the same as tabulated in refs. [3] and [6]. We have also made check calculations using the collisional rate coefficients of refs. [3] and [6] at a large number of other θ and η_e values, all of which agreed with the published values in [3] and [6] (however, note the misprints [24]: in ref. [6] $Z^3 K(1, 4)$ at θ = 32000 should read 7.44×10^{-11}, and in ref. [3] $X n_s(1) Z^{11}$ at θ = 32000, $\eta(c) = 10^{13}$ should read 5.5×10^9).

Acknowledgements

It is a pleasure to acknowledge Dr. F.E. Irons for his criticism of the manuscript and many helpful discussions.

References

[1] R.W.P. McWhirter, Plasma Diagnostic Techniques, ed. R.H. Huddlestone and S.L. Leonard (Academic Press, New York, 1965) pp. 201–264.
[2] J. Cooper, Rep. Progr. Phys. 29 (1966) 35.
[3] D.R. Bates, A.E. Kingston and R.W.P. McWhirter, Proc. Roy. Soc. A267 (1962) 297.
[4] D.R. Bates, A.E. Kingston and R.W.P. McWhirter, Proc. Roy. Soc. A270 (1962) 155.
[5] D.R. Bates and A.E. Kingston, Planet Space Sci. 11 (1963) 1.
[6] R.W.P. McWhirter and A.G. Hearn, Proc. Phys. Soc. 82 (1963) 641.
[7] A.G. Hearn, Proc. Phys. Soc. 88 (1966) 171.
[8] D.R. Bates, K.L. Bell and A.E. Kingston, Proc. Phys. Soc. 91 (1967) 288.
[9] H.W. Drawin, Z. Physik 225 (1969) 470; Z. Physik 225 (1969) 483.
[10] H.W. Drawin and F. Emard, Euratom Report, EUR-CEA FC-534 (1970).
[11] L.C. Johnson and E. Hinnov, J. Quant. Spectrosc. Radiat. Transfer 13 (1973) 333.
[12] A.A. Skorupski and S. Suckewer, J. Phys. B7 (1974) 1401.
[13] H.W. Drawin and F. Emard, Beiträge Plasma Phys. 15 (1975) 273.
[14] A. Burgess and H.P. Summers, Monthly Note Roy. Astron. Soc. 174 (1976) 345.
[15] H.W. Drawin, H. Quant. Spectrosc. Radiat. Transfer 10 (1970) 33.
[16] B.F. Gordiets, L.I. Gudzenko and L.A. Shelepin, J. Quant. Spectrosc. Radiat. Transfer 8 (1968) 791.

17] C.C. Limbaugh and A.A. Mason, Phys. Rev. A4 (1971) 2368.
18] W.L. Hogarth and D.L.S. McElwain, Proc. Roy. Soc. A345 (1975) 251; Proc. Roy. Soc. A345 (1975) 265.
19] W.W. Jones and A.W. Ali, Appl. Phys. Lett. 26 (1975) 450.
20] J.M. Green and W.T. Silfvast, Appl. Phys. Lett. 28 (1976) 253.
[21] G.J. Tallents, J. Phys. B (1977) accepted for publication.
[22] M.J. Seaton, Monthly Note Roy. Astron. Soc. 119 (1959) 81.
[23] W.L. Wiese, M.W. Smith and B.M. Glennon, Atomic Transition Probabilities, Vol. 1, Hydrogen through Neon (US Dept. of Commerce, 1966).
[24] R.W.P. McWhirter, personal communication (1976).

TEST RUN OUTPUT

```
 INPUT
 ZED     =     .1?000000E+01
 DNSTY   =     .1?000000E+15
 DEPTH   =                +0
 IM      =                +20
 EMP     =     .8?000000E+04
         =     .1?000000E+01

 END
 RCMOD
 KD      =     .00000000E+00,   .00000000E+00,   .00000000E+00,   .00000000E+00,
               .00000000E+00,   .00000000E+00,   .00000000E+00,   .00000000E+00,
               .00000000E+00,   .00000000E+00,   .00000000E+00,   .00000000E+00,
               .00000000E+00,   .00000000E+00,   .00000000E+00,   .00000000E+00,
               .00000000E+00,   .00000000E+00,   .00000000E+00,   .00000000E+00,
               .62E00000E-13,   .00000000E+00,   .00000000E+00,   .00000000E+00,
               .00000000E+00,   .00000000E+00,   .00000000E+00,   .00000000E+00,
               .00000000E+00,   .00000000E+00,   .00000000E+00,   .00000000E+00,
               .00000000E+00,   .00000000E+00,   .00000000E+00,   .00000000E+00,
               .00000000E+00,   .00000000E+00,   .00000000E+00,   .00000000E+00,
               .84100000E-15,   .15800518E-06,   .00000000E+00,   .00000000E+00,
               .00000000E+00,   .00000000E+00,   .00000000E+00,   .00000000E+00,
               .00000000E+00,   .00000000E+00,   .00000000E+00,   .00000000E+00,
               .00000000E+00,   .00000000E+00,   .00000000E+00,   .00000000E+00,
               .00000000E+00,   .00000000E+00,   .00000000E+00,   .00000000E+00,
               .13700000E-15,   .83495043E-08,   .35246350E-05,   .00000000E+00,
               .00000000E+00,   .00000000E+00,   .00000000E+00,   .00000000E+00,
               .00000000E+00,   .00000000E+00,   .00000000E+00,   .00000000E+00,
               .00000000E+00,   .00000000E+00,   .00000000E+00,   .00000000E+00,
               .00000000E+00,   .00000000E+00,   .00000000E+00,   .00000000E+00,
               .45562897E-16,   .17904530E-08,   .27638743E-06,   .15714776E-04,
               .00000000E+00,   .00000000E+00,   .00000000E+00,   .00000000E+00,
               .00000000E+00,   .00000000E+00,   .00000000E+00,   .00000000E+00,
               .00000000E+00,   .00000000E+00,   .00000000E+00,   .00000000E+00,
               .00000000E+00,   .00000000E+00,   .00000000E+00,   .00000000E+00,
               .19777458E-16,   .65737572E-09,   .68706300E-07,   .13819911E-05,
               .42023828E-04,   .00000000E+00,   .00000000E+00,   .00000000E+00,
               .00000000E+00,   .00000000E+00,   .00000000E+00,   .00000000E+00,
               .00000000E+00,   .00000000E+00,   .00000000E+00,   .00000000E+00,
               .00000000E+00,   .00000000E+00,   .00000000E+00,   .00000000E+00,
               .19475879E-16,   .31628978E-09,   .27054972E-07,   .36003282E-06,
               .38098297E-05,   .88725063E-04,   .00000000E+00,   .00000000E+00,
               .00000000E+00,   .00000000E+00,   .00000000E+00,   .00000000E+00,
               .00000000E+00,   .00000000E+00,   .00000000E+00,   .00000000E+00,
               .00000000E+00,   .00000000E+00,   .00000000E+00,   .00000000E+00,
               .62720210E-17,   .17838914E-09,   .13550939E-07,   .14508686E-06,
               .10030374E-05,   .80449483E-05,   .16325881E-03,   .00000000E+00,
               .00000000E+00,   .00000000E+00,   .00000000E+00,   .00000000E+00,
               .00000000E+00,   .00000000E+00,   .00000000E+00,   .00000000E+00,
               .00000000E+00,   .00000000E+00,   .00000000E+00,   .00000000E+00,
               .40793220E-17,   .11140526E-09,   .78318928E-08,   .73585440E-07,
               .40555376E-06,   .21101437E-05,   .14657081E-04,   .27429294E-03,
               .00000000E+00,   .00000000E+00,   .00000000E+00,   .00000000E+00,
               .00000000E+00,   .00000000E+00,   .00000000E+00,   .00000000E+00,
               .00000000E+00,   .00000000E+00,   .00000000E+00,   .00000000E+00,
               .28142160E-17,   .74711629E-10,   .49836436E-08,   .42926442E-07,
               .20603109E-06,   .84929388E-06,   .38071522E-05,   .24299713E-04,
               .43210292E-03,   .00000000E+00,   .00000000E+00,   .00000000E+00,
               .00000000E+00,   .00000000E+00,   .00000000E+00,   .00000000E+00,
               .00000000E+00,   .00000000E+00,   .00000000E+00,   .00000000E+00,
               .20313693E-17,   .52767028E-10,   .33888071E-08,   .27486407E-07,
               .12022251E-06,   .42958607E-06,   .15196332E-05,   .62394943E-05,
               .37733047E-04,   .64756432E-03,   .00000000E+00,   .00000000E+00,
               .00000000E+00,   .00000000E+00,   .00000000E+00,   .00000000E+00,
               .00000000E+00,   .00000000E+00,   .00000000E+00,   .00000000E+00,
               .15163591E-17,   .38794538E-10,   .24213770E-08,   .18795573E-07,
               .77052381E-07,   .24991271E-06,   .76355931E-06,   .24675188E-05,
               .95716803E-05,   .55765780E-04,   .93328374E-03,   .00000000E+00,
               .00000000E+00,   .00000000E+00,   .00000000E+00,   .00000000E+00,
               .00000000E+00,   .00000000E+00,   .00000000E+00,   .00000000E+00,
               .11642805E-17,   .29425885E-10,   .17975031E-08,   .13496900E-07,
               .52729796E-07,   .15969517E-06,   .44189369E-06,   .12303363E-05,
               .37489743E-05,   .13992307E-04,   .79337922E-04,   .13029374E-02,
```

```
                .000000000E+00,  .000000000E+00,  .000000000E+00,  .000000000E+00,
                .000000000E+00,  .000000000E+00,  .000000000E+00,  .000000000E+00,
                .91460559E-18,   .22887702E-10,   .13749918E-08,   .10058848E-07,
                .37898346E-07,   .10911730E-06,   .28138180E-06,   .70771046E-06,
                .18543402E-05,   .54267441E-05,   .19689612E-04,   .10945804E-03,
                .17714212E-02,   .000000000E+00,  .000000000E+00,  .000000000E+00,
                .000000000E+00,  .000000000E+00,  .000000000E+00,  .000000000E+00,
                .73221038E-18,   .18181989E-10,   .10771746E-08,   .77253599E-08,
                .28291714E-07,   .78337288E-07,   .19156495E-06,   .44836251E-06,
                .10598753E-05,   .26633194E-05,   .75705338E-05,   .26892543E-04,
                .14718471E-03,   .23548497E-02,   .000000000E+00,  .000000000E+00,
                .000000000E+00,  .000000000E+00,  .000000000E+00,  .000000000E+00,
                .59583063E-18,   .14702666E-10,   .86166989E-09,   .60765006E-08,
                .21751434E-07,   .58429183E-07,   .13721153E-06,   .30407929E-06,
                .66802978E-06,   .15130213E-05,   .36875259E-05,   .10252747E-04,
                .35838887E-04,   .19375807E-03,   .30705558E-02,   .000000000E+00,
                .000000000E+00,  .000000000E+00,  .000000000E+00,  .000000000E+00,
                .49159608E-18,   .12667533E-10,   .70021980E-09,   .48781255E-08,
                .17135593E-07,   .44921595E-07,   .10217584E-06,   .21711931E-06,
                .45113743E-06,   .94782443E-06,   .20812006E-05,   .49602518E-05,
                .13557585E-04,   .46784010E-04,   .25036044E-03,   .39370899E-02,
                .000000000E+00,  .000000000E+00,  .000000000E+00,  .000000000E+00,
                .41047502E-18,   .10034157E-10,   .53011264E-09,   .39817080E-08,
                .13775428E-07,   .35394698E-07,   .78456798E-07,   .16128000E-06,
                .32100567E-06,   .63766960E-06,   .12982196E-05,   .27833632E-05,
                .65146044E-05,   .17566993E-04,   .59962730E-04,   .31837072E-03,
                .49742202E-02,   .000000000E+00,  .000000000E+00,  .000000000E+00,
                .34651663E-18,   .84371019E-11,   .48304281E-09,   .32931954E-08,
                .11260973E-07,   .28468049E-07,   .61753472E-07,   .12360398E-06,
                .23781367E-06,   .45210817E-06,   .86896731E-06,   .17269357E-05,
                .36348058E-05,   .83907764E-05,   .22376623E-04,   .75733931E-04,
                .39921700E-03,   .62029324E-02,   .000000000E+00,  .000000000E+00,
                .29520515E-18,   .71646456E-11,   .40827718E-09,   .27598843E-08,
                .93368411E-08,   .23281344E-07,   .49627748E-07,   .97495212E-07,
                .18182771E-06,   .33391103E-06,   .61402334E-06,   .11514683E-05,
                .22445131E-05,   .46569815E-05,   .10626501E-04,   .28077168E-04,
AKION =         .94319821E-04,   .49441160E-03,   .76454295E-02,   .000000000E+00
                .49000000E-16,   .45061632E-08,   .15720050E-06,   .72944741E-06,
                .17769257E-05,   .32568115E-05,   .51268867E-05,   .73592872E-05,
                .99368557E-05,   .12849008E-04,   .16089067E-04,   .19652703E-04,
                .23537033E-04,   .27740083E-04,   .32260470E-04,   .37097204E-04,
                .42249565E-04,   .47717016E-04,   .53499152E-04,   .59595664E-04
AKREC =         .000000000E+00,  .000000000E+00,  .000000000E+00,  .000000000E+00,
                .000000000E+00,  .000000000E+00,  .000000000E+00,  .000000000E+00,
                .000000000E+00,  .000000000E+00,  .000000000E+00,  .000000000E+00,
                .000000000E+00,  .000000000E+00,  .000000000E+00,  .000000000E+00,
                .000000000E+00,  .000000000E+00,  .000000000E+00,  .000000000E+00
$END
```

H-LIKE ION DENSITY DATA

N	RO(N)	R1(N)	SAHA-BOLTZMANN DENSITIE (CM**-3)
1			2.188+15
2	3.35-02	8.58-03	3.262+09
3	6.06-01	2.65-03	4.734+08
4	8.68-01	8.51-04	3.224+08
5	9.51-01	3.15-04	3.232+08
6	9.79-01	1.33-04	3.656+08
7	9.90-01	6.26-05	4.303+08
8	9.95-01	3.22-05	5.114+08
9	9.97-01	1.77-05	6.066+08
10	9.98-01	1.03-05	7.150+08
11	9.99-01	6.23-06	8.361+08
12	9.99-01	3.91-06	9.694+08
13	1.00+00	2.52-06	1.115+09
14	1.00+00	1.65-06	1.272+09
15	1.00+00	1.09-06	1.442+09
16	1.00+00	7.19-07	1.623+09
17	1.00+00	4.67-07	1.816+09
18	1.00+00	2.92-07	2.021+09
19	1.00+00	1.67-07	2.238+09
20	1.00+00	7.49-08	2.467+09

C-R RECOMBINATION COEFF 7.63-12 CM**3 S**-1
C-R IONIZATION COEFF 2.12-15 CM**3 S**-1

ATOMIC NUMBER 1.00
ELECTRON DENSITY 1.000+14 CM**-3
LDEPTH = 0
ELECTRON TEMPERATURE 8.000+03 DEGREES K
X = 1.00

NORMAL EXIT. EXECUTION TIME: 1228 MILLISECONDS.

APPENDIX B

An Adjustable Slit Mechanism

Commercial slit mechanisms, and those described in the literature (eg Sears 1933, Barnes and Brattain 1935, Strong 1941, White and Liston 1950, Jones 1952, 1956) are not particularly suitable for the 45° PPEA since they are either limited in slit width range (only up to 1 mm normally), or cannot accept beams at 45° to the slit jaws (because the slit mechanism is directly behind the jaws). We have consequently designed an adjustable slit mechanism especially for use with our 45° PPEA. Briefly (see Figure App. B.1), the slit mechanism comprises a left and right handed brass leadscrew (1) (numbers refer to Figure App. B.1) of 40 turns per inch (≃1.57 turns per mm) carrying left and right hand threaded aluminium yokes (2 and 3) which in turn carry jaw plates (4 and 5) to which the (stainless steel) slit jaws (6) are attached. The yokes are adjustable to enable back lash in the threads to be eliminated. The leadscrew is driven by a 40:1 reduction worm gear (7), and the leadscrew and worm are mounted on small ball bearings lubricated with "Apiezon 100AP" PTFE loaded vacuum grease. A stop (not shown) mounted on the leadscrew was positioned to prevent an operator closing the slit jaws onto themselves. The worm (7) is driven through a bellows coupling (8) by a calibrated turn counting knob (10) outside the vacuum. A gasket seal

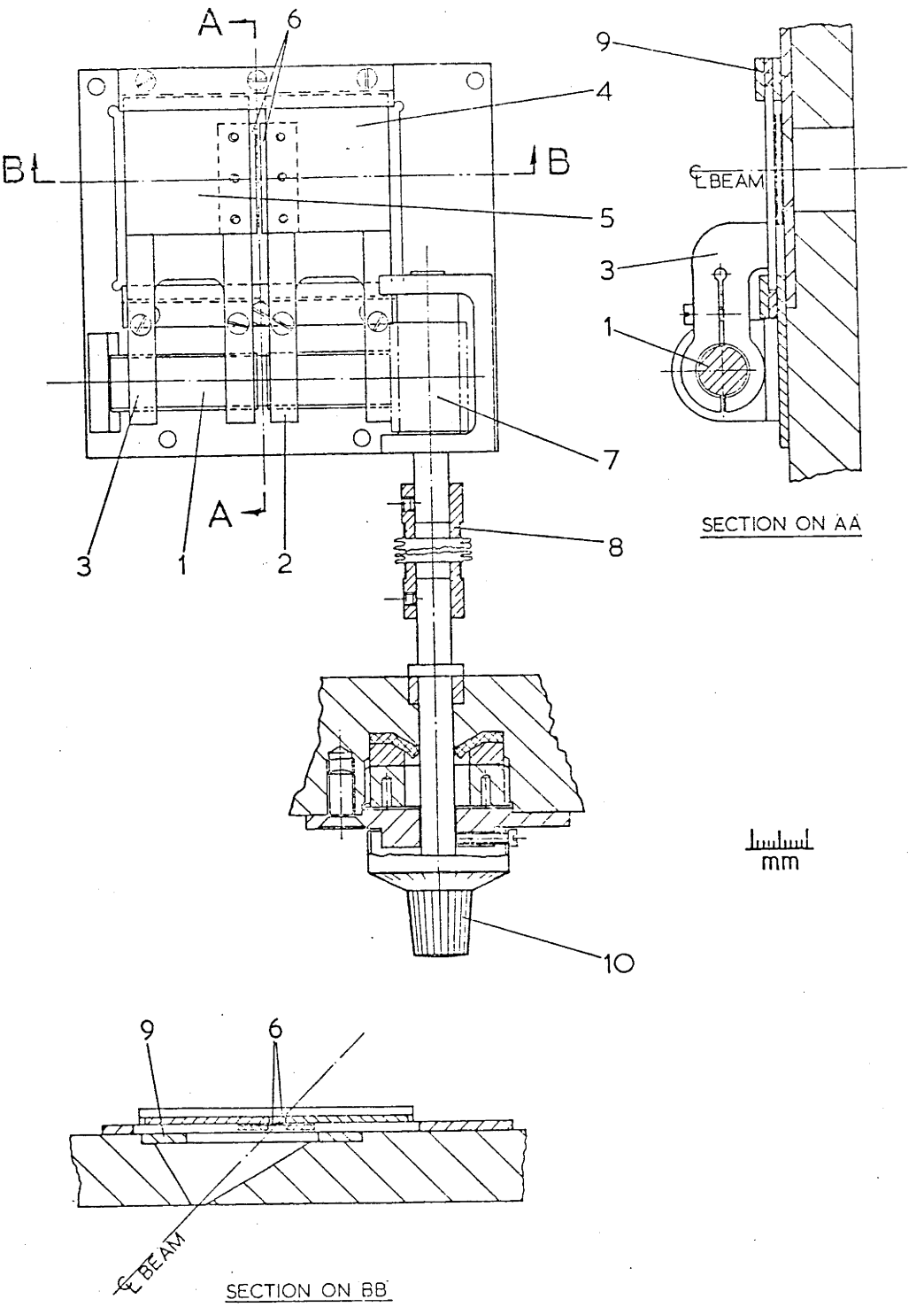

Figure App.B.1: The adjustable slit mechanism as attached to the ground plate of the analyzer. The numbered components are identified in the text.

(Wilson 1941) is used for the vacuum feed through. The height of the slit can be varied by replacing the gate (9) when the mechanism is up to atmospheric pressure. The slit width is continuously adjustable from about 0.02 mm (depending on the position of the stop) up to 2.5 mm, with an accuracy estimated by closing the slit jaws onto foils of standard thickness, within ± 0.005 mm.

REFERENCES

Afanas'ev Yu V and Rozanov V B (1972), Sov. Phys. JETP 35, 133-5.

Ali A W and Jones W W (1976), Phys. Lett. 55A, 462-4.

Allen F J (1970), J. Appl. Phys. 41, 3048-51.

_____ (1971), Rev. Sci. Instr. 42, 1423-7.

_____ (1972), J. Appl. Phys. 43, 2169-75.

Barnes R B and Brattain R R (1935), Rev. Sci. Instr. 6, 83-4.

Basov N G, Krokhin O N and Sklizkov G V (1967), Appl. Opt. 6, 1814-17.

Bates D R, Kingston A E and McWhirter RWP (1962), Proc. R. Soc. A 267, 297-312.

Bohn W L (1971), Proc. 10th Int. Conf. on Phenomena in Ionized Gases, Oxford (Oxford: Parsons), p. 386.

_____ (1974), Appl. Phys. Lett 24, 15-7.

Boland B C, Irons F E and McWhirter RWP (1968), J. Phys. B: Atom. Molec. Phys. 2, 1180-91.

Bruce C W, Deacon J and Vonderhaar D F (1966), Appl. Phys. Lett. 9, 164-6.

Bryce P, Dalglish R L and Kelly J C (1973), Can. J. Phys. 51, 574-86.

Bushuev V A and Kuz'min R N (1975), Sov. Phys.-Usp. 17, 942-9.

Bykovskii Yu A et al. (1970), Sov. Phys.-Tech. Phys. 14, 1269-71.

_____ (1971a), Sov. Phys. JETP 33, 706-12.

_____ (1971b), JETP Lett. 14, 157-9.

Caruso A and Gratton R (1968), Plasma Phys. 10, 867-77.

Chapline G and Wood L (1975), Physics Today (June), pp. 40-8.

Chapline G and Wood L (1976), Sov. J. Quant. Elect. 6, 452-4.

Charatis G et al. (1974), Proc. 5th IAEA Conf. Plasma Phys. and Controlled Nuclear Fus. Res. Tokyo (Vienna, IAEA), pp. 317-33.

Chowdhury S S and Miles H T (1971), Report for Research Contract AGMT/CUL/786 Dept. of Physics, Univ. College of Swansea, Univ. of Wales.

Christiansen J P, Ashby DETF and Roberts K V (1974), Comput. Phys. Commun. 7, 271-87.

_____ (1975), Comput. Phys. Commun. 10, 251-6.

Dalglish R L and Kelly J C (1976), J. Phys. D: Appl. Phys. 9, 581-92.

David C D (1967), Appl. Phys. Lett. 11, 394-6.

Dawson J M (1964), Phys. Fluids 7, 981-7.

Decoste R and Ripin B H (1977), Appl. Phys. Lett. 31, 68-70.

Demtröder W and Jantz W (1970), Plasma Phys. 12, 691-703.

Dewhurst R J, Jacoby D, Pert G J and Ramsden S A (1976), Phys. Rev. Lett. 37, 1265-8.

Dick K et al. (1973), J. Appl. Phys. 44, 3284-93.

Donaldson T P, Hutcheon R J and Key M H (1973), J. Phys. B: Atom. Molec. Phys. 6, 1525-44.

Drawin H W (1969), Z. Naturforsch. 24a, 1492-6.

_____ (1970), J. Quant. Spectrosc. Radiat. Transfer 10, 33-48.

Drawin H W and Emard F (1970), Euratom Report EUR-CEA-FC-534.

Drawin H W, Emard F and Katsonis K (1973), Z. Naturforsch 28a, 1422-31.

Ehler A W (1975), J. Appl. Phys. 46, 2464-7.

Fauquignon C and Floux F (1970), Phys. Fluids 13, 386-91.

Fawcett B C (1971), J. Phys. B: Atom. Molec. Phys. 4, 981-5.

Fawcett B C, Galanti M and Peacock N J (1974), J. Phys. B: Atom. Molec. Phys. 7, 1149-53.

Fleischmann H H, Ashby DETF and Larson A V (1965), Nucl. Fus. 5, 349-51.

François R and Barat M (1968), C.R. Acad. Sc. Paris B266, 1306-8.

Galanti M and Peacock N J (1975), J. Phys. B: Atom. Molec. Phys. 8, 2427-47.

Gillman G B (1977), J. Phys. E: Sci. Instrum. 10, 959-60.

Goforth R R (1975), Appl. Phys. Lett. 27, 598-600.

_____ (1976), Rev. Sci. Instr. 47, 548-52.

Goforth R R and Hammerling P (1976), J. Appl. Phys. 47, 3918-22.

Gol'dfarb V M and Luk'yanov G A (1969), Sov. Phys.-Tech. Phys. 13, 1365-9.

Gordiets B F, Gudzenko L I and Shelepin L A (1968), J. Quant. Spectrosc. Radiat. Transfer 8, 791-804.

Gorog I (1968), Phys. Lett. 28A, 371-2.

Green T S (1970), Plasma Phys. 12, 877-83.

Green T S and Proca G A (1970), Rev. Sci. Instr. 41, 1409-14.

Green J M and Silfvast W T (1976), Appl. Phys. Lett. 28, 253-5.

Gregg D W and Thomas S J (1966), J. Appl. Phys. 37, 4313-6.

Griem H R (1964), "Plasma Spectroscopy" (New York: McGraw-Hill), p. 166.

_____ (1974), "Spectral Line Broadening by Plasmas" (New York: Academic), p. 8.

Gudzenko L I and Shelepin L A (1965), Sov. Phys.-Dokl. 10, 147-9.

Gudzenko L I, Shelepin L A and Yakovlenko S I (1975), Sov. Phys.-Usp. 17, 848-63.

Gurevich A V and Pitaevskii L P (1964), Sov. Phys. JETP 19, 870-1.

Harrower G A (1955), Rev. Sci. Instr. 26, 850-4.

Haught A F and Polk D H (1966), Phys. Fluids 9, 2047-56.

Hoffmann P and Bohn W L (1972), Z. Naturforsch 27a, 878-80.

Honig R E (1963), Appl. Phys. Lett. 3, 8-11.

Hora H (1969), Phys. Fluids 12, 182-91.

_____ (1975), J. Opt. Soc. Am. 65, 882-6.

_____ (1976), Sov. J. Quantum. Electron. 6, 154-9.

Irons F E (1973), J. Phys. B: Atom. Molec. Phys. 6, 1562-81.

_____ (1975), J. Phys. B: Atom. Molec. Phys. 8, 3044-68.

_____ (1976), J. Phys. B: Atom. Molec. Phys. 9, 2737-53.

Irons F E, McWhirter RWP and Peacock N J (1972), J. Phys. B: Atom. Molec. Phys. 5, 1975-87.

Irons F E and Peacock NJ (1974a), J. Phys. B: Atom. Molec. Phys. 7, 1109-12.

_____ (1974b), J. Phys. B: Atom. Molec. Phys. 7, 2084-99.

Jaeglé P, Jamelot G, Carillon A and Sureau A (1976), Report presented at 4th Workshop "Laser interaction and related plasma phenomena", RPI Troy New York, Nov. 8-12, 1976.

Jones R V (1952), J. Sci. Instr. 29, 345-50.

_____ (1956), J. Sci. Instr. 33, 169-73.

Jones W W and Ali A W (1975), Appl. Phys. Lett. 26, 450-1.

Kang H B et al. (1972), Japan. J. Appl. Phys. 11, 765-6.

_____ (1973), J. Phys. Soc. Japan 34, 504-12.

Kuznetsov N M and Raizer Yu. P (1965), Z. Priklad. Mekhan. Tech. Fiz. 4, 10-20.

Langer P, Tonon G, Floux F and Ducauze A (1966), IEEE J. Quant. Elect. QE-2, 499-506.

Linlor W I (1963), Appl. Phys. Lett. 3, 210-11.

Luther-Davies B (1977), Opt. Commun. 23, 98-104.

Marr G V (1968), "Plasma Spectroscopy" (Amsterdam: Elsevier), p. 276.

Mason D W (1964), Plasma Phys. 6, 553-8.

Mattioli M (1971), Plasma Phys. 13, 19-28.

McWhirter RWP and Hearn A G (1963), Proc. Phys. Soc. 82, 641-54.

McWhirter RWP (1965), "Plasma Diagnostic Techniques", ed. R H Huddlestone and S L Leonard (New York: Academic), Chapter 5.

Mulser P (1971), Plasma Phys. 13, 1007-12.

Nuckolls J, Wood L, Thiessen A and Zimmerman G (1972), Nature 239, 139-42.

Olsen J N, Kuswa G W and Jones E D (1973), J. Appl. Phys. 44, 2275-83.

Opower H and Burlefinger E (1965), Phys. Lett. 16, 37-8.

Opower H and Press W (1966), Z. Naturforsch. 21a, 344-50.

Oron M and Paiss Y (1973), Rev. Sci. Instrum. 44, 1293-6.

Paton B E and Isenor N R (1966), Can. J. Phys. 46, 1237-9.

Peacock N J and Pease R S (1969), J. Phys. D: Appl. Phys. 2, 1705-16.

Proca G A and Green T S (1970), Rev. Sci. Instr. 41, 1778-83.

Puell H (1970), Z. Naturforsch 25a, 1807-15.

Puell H, Neusser H J and Kaiser W (1970), Z. Naturforsch. 25a, 1815-22.

Ready J F (1963), Appl. Phys. Lett. 3, 11-13.

Rumsby P T and Paul JWM (1974), Plasma Phys. 16, 247-60.

Salzmann H (1973), J. Appl. Phys. 44, 113-24.

Sears J E (1933), J. Sci. Instr. 10, 376-7.

Siegrist M R (1976), Opt. Commun. 16, 402-7.

Sklizkov G V (1971), "Laser Interaction and Related Plasma Phenomena", ed. H J Schwarz and H Hora (New York: Plenum), p. 255.

Skorupski A A and Suckewer S (1974), J. Phys. B: Atom. Molec. Phys. 7, 1401-10.

Spitzer L (1956), "Physics of Fully Ionized Gases" (New York: Interscience).

Strong J (1941), Rev. Sci. Instr. 12, 213-4.

Suckewer S, Hawryluk R J, Okobayashi M and Schmidt J A (1976), Appl. Phys. Lett. 29, 537-9.

Tonon G F (1972), IEEE Trans. Nucl. Sc. NS-19, 172-83.

Tonon G and Rabeau M (1973), Plasma Phys. 15, 871-82.

Tonon G, Schirmann D and Rabeau M (1971), Proc. 10th Int. Conf. on Phenomena in Ionized Gases, Oxford (Oxford: Parsons), p. 225.

Waynant R W and Elton R C (1976), Proc. IEEE 64, 1059-92.

White J V and Liston M D (1950), J. Opt. Soc. Am. 40, 29-35.

Wilson R R (1941), Rev. Sci. Instr. 12, 91-3.

Yarnold G D and Bolton H C (1949), J. Sci. Instr. 26, 38-40.

Zel'dovich Ya B and Raizer Yu P (1967), "Physics of Shock Waves and High Temperature Hydrodynamic Phenomena" (New York: Academic), pp. 573-9.

The references for Appendix A are not included in the above list.

LIST OF SYMBOLS

Symbol	Representing	Introduced in Section No.
$A(n, m)$	the radiative transition probability from state $n \rightarrow m$ in a hydrogen-like ion	2.2
d	the distance between the deflecting and ground plates of the PPEA	4.4.1
E	a constant which takes account of the spectral line profile when calculating small signal gain due to stimulated emission at line centre	2.3.5
E	ion kinetic energy	4.4.1
E_p	the ion energy where $n_Z(E)$ or $N(E)$ peaks	5.3
e	charge on the electron	4.4.2
F_e	electron thermal conduction flux assuming many mean free paths for conduction	2.4.1
$(F_e)_{max}$	free streaming electron thermal conduction flux	2.4.1
F_e^l	the assumed MEDUSA electron thermal conduction flux	2.4.1
$G(n, m)$	the small signal gain due to stimulated emission at line centre for a transition from state $n \rightarrow m$	2.3.5
I	peak current detected for an ion species with the PPEA	4.4.2
I	laser intensity on target	5.2
$K(c, n)$	the rate coefficient for three-body recombination from the continuum c to state n of a hydrogen-like ion	2.2

$K(n, c)$	the rate coefficient for collisional ionization from state n of a hydrogen-like ion to the continuum c	2.2
$K(n, m)$	the rate coefficient for a collision-induced transition from state $n \rightarrow m$ in a hydrogen-like ion	2.2
k_1, k_2	constants	5.3
k	Boltzmann's constant	6.3.2
L_α	symbol for Lyman alpha	2.2
M	atomic weight	2.4.2
m	a principal quantum number	2.2
m_i	ion mass	6.2
N_n	number density of quantum state n of hydrogen-like ions	2.2
N^z	number density of fully stripped ions	2.2
N_e	free-electron density	2.2
$N(E)$	the energy density of ions entering the PPEA entrance slit	4.4.2
$N(v)$	the velocity density of ions entering the PPEA entrance slit	6.2.1
n	principal quantum number	2.2
n^*	a hydrogen-like ion quantum state selected so that the population densities of states $n \leq n^*$ are computed time-dependently, while states $n > n^*$ are treated as being quasi-steady state	2.2.2
n_ℓ	lower quantum state	2.3.5
n_u	upper quantum state	2.3.5
$n_s(1)$	number density of ground state hydrogen-like ions in the steady state	2.2

$n_Z(E)$	the energy density per unit volume of ions of charge Z and energy E at the PPEA entrance slit	5.3
r_0	initial plasma radius	2.4.2
T	plasma temperature	2.4.2
T_e	electron temperature	2.2.1
T_e^{ts}	T_e at the target surface	6.3.2
T_i	ion temperature	2.4.2
T_t	ion translation temperature	6.3.2
$T_{1/2}$	electron temperature half-life	2.2.2
T	probability that a L_α photon propogates an optical depth τ	3.2
t	time	2.2
t_r	recombination time constant	6.3.1
V	deflecting plate potential in the PPEA	4.4.1
v_ℓ	ion velocity determined using luminosity time-of-flight	6.2.2
v_p	ion velocity where N(v) peaks	6.2.1
v_s	ion acoustic speed	2.4.2
W_{ent}	PPEA entrance slit width	4.4.1
W_{exit}	PPEA exit slit width	4.4.1
W_{ent}^{max}	entrance slit widths larger than W_{ent}^{max} result in saturation of the PPEA output signal	5.2
X $(= N_e/N^Z)$	the ratio of electron density to fully stripped ion density	2.2
x	distance from the entrance to the exit slit of the PPEA	4.4.1
Z	ion charge	4.4.1
Z	atomic number	2.1

α	recombination rate coefficient	6.3.1
$\beta(n)$	the two-body recombination coefficient to the state n in a hydrogen-like ion	2.2
γ	the ratio of specific heat at constant pressure to that at constant volume	6.3.2.1
ΔE	energy bandwidth	4.4.1
$\Delta\nu$	spectral line full half-width	2.3.5
ε_0	permittivity of free space	5.3
η_e $(= N_e/Z^7)$	reduced electron density	3.2
$\eta(c)$ $(=N_e/Z^7)$	" " "	2.2
η_n $(= N_n X/Z^{11})$	reduced population density of quantum state n	3.2
η_1^{max}	the maximum hydrogen-like ion ground state density which can be tolerated and still achieve a $3 \rightarrow 2$ inversion	3.3
θ $(= T_e/Z^2)$	reduced electron temperature	2.2
$\Lambda(n, m)$	the optical escape factor for the transition $n \rightarrow m$ in a hydrogen-like ion	2.2
λ	wavelength	2.3.5
ν	frequency	2.3.5
ν_0	frequency at line centre	2.3.5
τ	optical depth	3.2
$\chi(n, m)$	energy separation of hydrogen-like ion quantum state n and m	3.3
ω_n	the statistical weight of quantum state n	2.3.1

Symbols used only in Appendix A are not included in the above list.